Journal of Marine Systems 109–110 (2013) S3–S25

Contents lists available at SciVerse ScienceDirect

Journal of Marine Systems

journal homepage: www.elsevier.com/locate/jmarsys

Modelling the barotropic tide along the West-Iberian margin

Luis S. Quaresma [a,*], Annick Pichon [b]

[a] INSTITUTO HIDROGRAFICO, Divisão de Oceanografia, Rua das Trinas, nº49, 1249–093 Lisboa, Portugal
[b] SHOM, HOM/REC, 13 rue du Chatellier, 29200 Brest, France

ARTICLE INFO

Article history:
Received 1 October 2010
Received in revised form 5 August 2011
Accepted 21 September 2011
Available online 10 October 2011

Keywords:
Barotropic tide
Barotropic forcing term
Numerical model
Tide-gauge
ADCP data

ABSTRACT

The present work explores the use of a numerical model to predict the barotropic tide along the West-Iberian region, extending from the Gulf of Cadiz to the Bay of Biscay and from the shelf to nearby seamounts (Gorringe and Galicia banks). The model is used, in a single isopycnal layer, to simulate the 2D propagation of the following eight principal tidal constituents: M2, S2, N2, K2, K1, O1, P1 and Q1. Astronomical tide-raising force is introduced into the equations of motion in order to improve model results. Recently updated global tide solutions are optimally combined to force a polychromatic tidal spectrum at the open boundaries. New bathymetry is built from hydrographic databases and used to increase the accuracy of the model, especially over the Portuguese continental shelf. Data from several tide gauges and acoustic Doppler current profilers are used to validate the numerical solution. Tidal amplitude and tidal current velocity solutions are evaluated by classical harmonic analysis of *in situ* and simulated time-series. Model outputs demonstrate the improvement of the regional hydrodynamic tide solution from earlier references. The harmonic solutions highlight small-scale variability over the shelf, and over nearby seamounts, due to the generation of diurnal continental shelf waves and topographic modulation of the semi-diurnal tidal ellipses. The barotropic forcing term is calculated over the study region and the main internal tide generation "hotspots" are revealed.

1. Introduction

The West-Iberian margin is marked by a narrow continental shelf shaped by submarine canyons, promontories and capes (Fig. 1). Its major topographic feature is the Estremadura promontory, extending 200 km offshore and forming a wide shallow plateau (Tagus Plateau). Two important submarine canyons (Nazaré and Setúbal) delimit this structure and increase its slope at the north and south faces. These topographic features divide a wider shelf to the north from an almost absent shelf to the south. Other smaller canyons, seamounts (Gorringe and Galicia banks) and islands increase the intricacy of this region.

Different oceanographic processes occur in the region, varying in spatial and time scales. A common shelf/slope current velocity power spectrum shows an energetic band at tidal frequencies, bounded by low-frequency circulation and energetic high-frequency activity. The low-frequencies domain highlights the deep/subsurface poleward thermohaline flows, as well as frequent wind-driven transport. During winter, the short-period processes are dominated by storm gravity waves and during summer by non-linear internal tide dynamics (Quaresma et al., 2007).

As far as tidal dynamics are concerned, the M2 semi-diurnal constituent is dominant over the study region. The S2 is the next-largest constituent and consequently introduces Spring-Neap tidal modulation along the continental shelf. N_2 and K_2 harmonics are also very energetic, being responsible for longer period modulation. While being less energetic, the O_1 and K_1 diurnal constituents are also present and are responsible for the observed diurnal inequality of the tide. These six principal tidal harmonics are then followed by five semi-diurnal waves ($2N_2$, MU_2, NU_2, L_2, T_2) and by two other diurnal constituents, Q_1 and P_1 (Fig. 2). Within the same order of amplitude, the study region also reveals long-period radiational harmonics (SA, SSA and MM). Although the observed tidal currents are small (rarely above 0.2 $m.s^{-1}$), when compared with other coastal regions, they are the driving force of the strong high-frequency baroclinic activity, recorded over this margin (Azevedo et al., 2006; Da Silva et al., 1998; Jeans and Sherwin, 2001; Quaresma et al., 2007; Sherwin et al., 2002; Small, 2002).

To understand and predict the complex dynamics of the regional internal tidal features, the MITIC research project (Modelling of the Internal Tide over the West-Iberian Coastal margin) was put together in a partnership between the Portuguese and the French hydrographic offices (HIDROGRAFICO and SHOM). The study of the internal tide dynamics requires knowledge and accurate forecasting of the barotropic tidal solution. This task was explored in the present work by the use of HYCOM (HYbrid Coordinate Ocean Model), in a 2D tidal hydrodynamic regional configuration.

Other authors have dedicated work to model the barotropic tide over this continental margin. Among them, it is important to point out studies performed by Fanjul et al. (1997), who applied a 3D Z-coordinate model (HAMSOM) with a variable grid size scheme.

* Corresponding author. Tel.: +351 210943000.
E-mail address: luis.quaresma@hidrografico.pt (L.S. Quaresma).

0924-7963/$ – see front matter © 2011 Elsevier B.V. All rights reserved.
doi:10.1016/j.jmarsys.2011.09.016

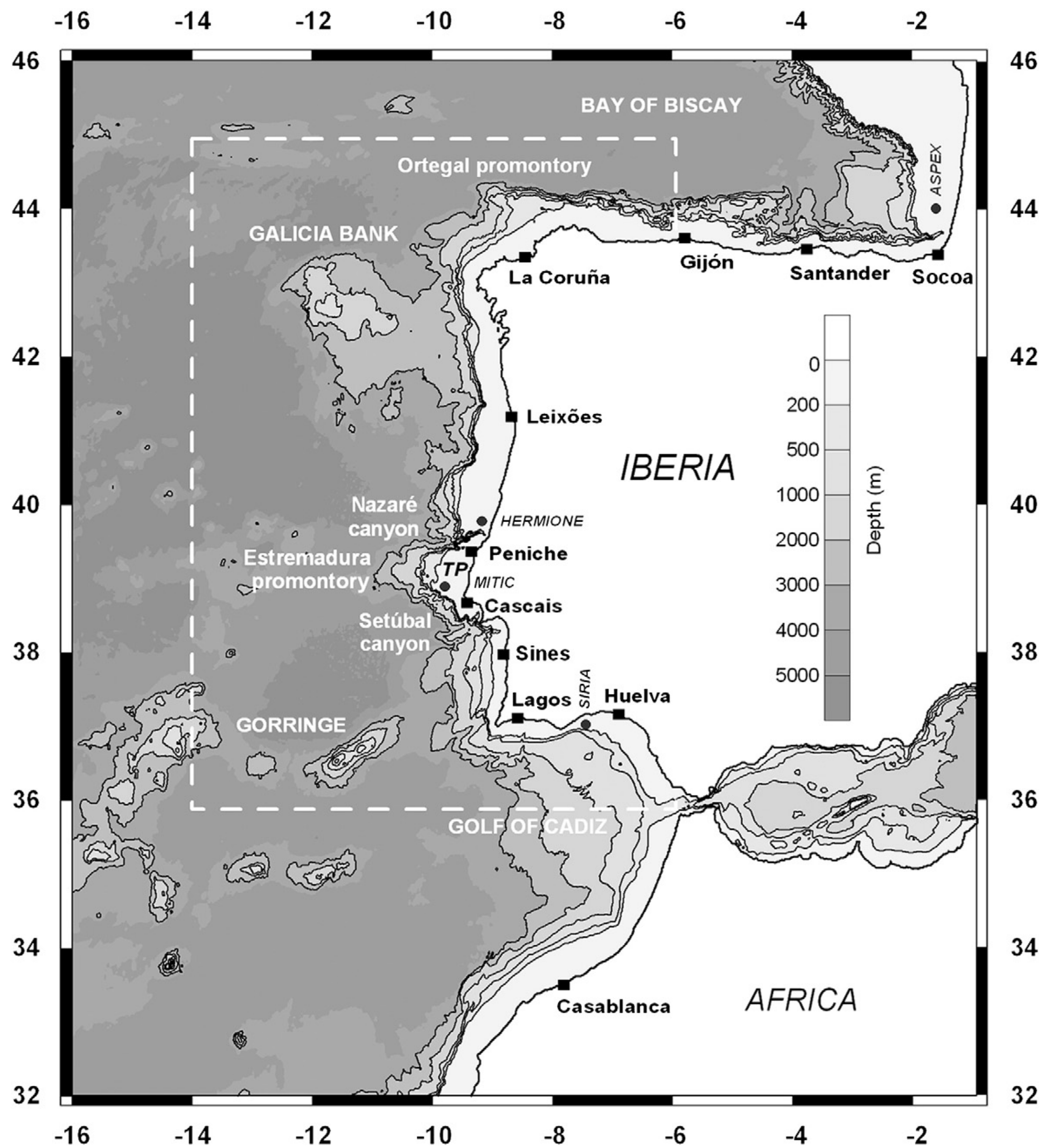

Fig. 1. The West-Iberian region (numerical model domain). Global tide solutions were forced at the open boundaries. These limits were selected in order to guarantee a homogeneous deep-ocean condition (distant from important topographic structures). Black squares indicate tide-gauges and gray circles the current-profile dataset locations, used to validate model results. The white dashed line delimits the study domain.

Monochromatic tidal waves, derived from the first TOPEX/POSEIDON datasets, were forced at the open boundaries. The simulation suggests Kelvin wave mode propagation, from south to north with amplitudes increasing towards the coast. Extensive solution validation was performed by tide-gauge data. Sauvaget et al. (2000) used TELEMAC-2D to model these structures, zooming the northern Portuguese shelf. A special attention was given to M2 and K1 constituents, revealing the generation of diurnal continental shelf waves trapped at the shelf. Fortunato et al. (2002) dedicated a full article to discuss these phenomena, by using a finite element model (ADCIRC). Their study pointed out the Tagus Plateau's responsibility as the trapped wave trigger. Recently, Marta-Almeida and Dubert (2006) applied the ROMS model to the same region in order to show the structure of eight principal tide harmonics (M2, S2, N2, K2, K1, O1, P1 and Q1) over the northern Portuguese shelf. This study reinforced the strong topographic effect of the Tagus Plateau in the reshaping of the diurnal solution (intensification of surface elevation and current magnitude, as well as the modulation of their phase velocity).

The originality of the present work was the simulation of a polychromatic tidal spectrum to obtain a regional tide solution. Eight principal constituents, essential to reproduce the regional tide behaviour, were assembled and forced at the open boundaries. This option allows non-linear harmonic interactions in the resulting solution, as expected in nature. Other authors frequently adopt a monochromatic methodology in short period model runs to reduce numerical costs and avoid uncontrolled constituent interactions. The present model outputted an absolute tidal solution and its evaluation was performed by harmonic analysis. Higher accuracy was achieved by adding the gravitational tidal gradient force into HYCOM momentum equations and by improving the bathymetric information over the region. Self-attraction/loading (SAL) terms were not included, based on the principle that they are negligible near coastal regions and that the utility

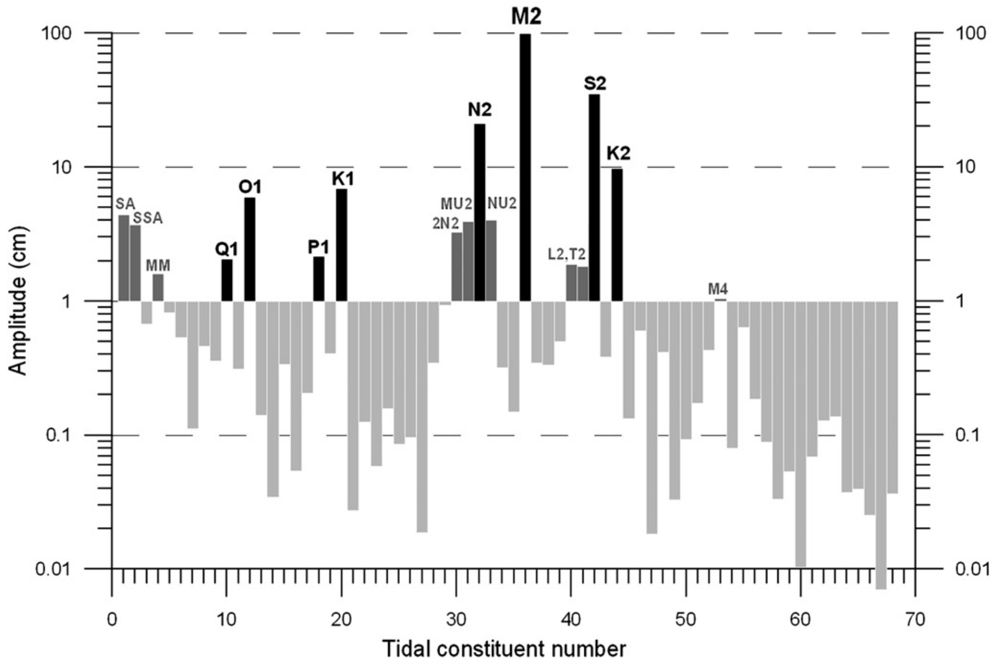

Fig. 2. Tidal constituents at Cascais tide gauge (Portugal). The amplitude was obtained by harmonic analysis of 4 years record. The length of the used time-series allows the extraction of 68 constituents. The y-axis divides the constituents with amplitudes higher than 1 cm from all the others. Notice that the eighth modelled constituents are not the most energetic. Other semi-diurnal harmonics (2N2, MU2, NU2, L2 and T2) have the same order of magnitude as Q1 and P1. Radiational harmonics are also present with relevant energy (SA, SSA and MM).

of adopting them is questionable (Ray, 1998). Finally, an effort was made to validate both sea-surface height and tidal current velocity solutions for each constituent. Accurate barotropic tidal ellipse simulations enabled better estimations of the internal tide generation forcing term, as done by Pichon and Correard (2006).

In Section 2, *in situ* observation datasets are presented. The numerical model is briefly introduced, focusing on momentum and continuity equations. The viscosity parameterization in the model is also considered. A new bathymetry is proposed and two different global tide solutions are discussed.

Model results are validated in Section 3 by tide-gauge records and current profile datasets. The barotropic structure of the tide is illustrated and analysed in Section 4. A general description is made for diurnal and semi-diurnal constituents, using the K1 and M2 harmonics as representatives of each sub and super-inertial forcing group. A specific discussion is dedicated to the small-scale shelf variability observed along the West-Iberian margin (Section 5). In Section 6 the barotropic forcing term is calculated over the study region and the main internal tide generation “hotspots” are identified.

2. Materials and methods

2.1. Data analysis

Several sea-level records and mid-shelf current profiles were made available for the present study (see Tables 1 and 2). They were used to validate model results and to help its parameterization. Data are the property of the following institutions: HIDROGRAFICO (Portuguese Hydrographic Office and Marine National Laboratory, PT), SHOM (French Hydrographic Office, FR1), IFREMER (French Marine National Laboratory, FR2) and PUERTOS DEL ESTADO (Spanish National Harbours Office, ES). Tide gauges were selected by location criteria. They are spaced along the domain and reflect, as much as possible, the offshore tide solution. The adopted model spatial resolution (1-arc minute) restrained the desirable representation of coastal inlets. This constraint advised the discard of tide gauges placed inside estuaries and inside the Galician Rias. Nodal corrections were applied to amplitude and phase estimations. No correction was made for atmospheric effects.

Tide-gauge data was re-sampled hourly and submitted to classical harmonic analysis, using the available open source tool T_TIDE (Pawlowicz et al., 2002). This option allows other authors to repeat the present analysis and perform equivalent evaluations. Different years and record lengths were used, based on data availability and data quality. These requisites ensure the absence of large holes (invalid data) in the employed time series, enabling coherent harmonic analysis. Exception is made to PUERTOS DEL ESTADO data, where

Table 1
Tide-gauge datasets location and record lengths. FR1 stands for SHOM, ES for PUERTOS DEL ESTADO and PT for HIDROGRAFICO. Tide-gauge technology is present in System column. The dataset from Casablanca tide-gauge was taken from SHOM's database.

Site		Position (WGS-84)		System	Record length (years)	Period
St Jean-de-luz (Socoa)	FR1	43° 23′ 42.0″ N	1° 40′ 54.0″ W	Radar	3	2007–2009
Santander	ES	43° 27′ 45.0″ N	3° 47′ 22.0″ W	Ultrasonic	7	1993–2000
Gijón	ES	43° 33′ 33.0″ N	5° 41′ 50.0″ W	Ultrasonic	4	1996–2000
Coruña	ES	43° 21′ 31.0″ N	8° 23′ 17.0″ W	Ultrasonic	6	1993–1999
Leixões	PT	41° 11′ 07.8″ N	8° 42′ 14.0″ W	Float gauge	3.5	2005–2008
Peniche	PT	39° 21′ 13.5″ N	9° 21′ 28.2″ W	Pressure	2	2007–2008
Cascais	PT	38° 41′ 35.4″ N	9° 24′ 55.4″ W	Float gauge	3	2004–2006
Sines	PT	37° 56′ 53.4″ N	8° 53′ 16.2″ W	Float gauge	3	2006–2008
Lagos	PT	37° 05′ 56.0″ N	8° 40′ 06.0″ W	Float gauge	3	2000–2002
Huelva	ES	37° 07′ 56.0″ N	6° 50′ 02.0″ W	Ultrasonic	3	1997–2000
Casablanca	FR1	33° 36′ 46.0″ N	7° 36′ 19.8″ W	Float gauge	0.5	2005

Table 2
ADCP current profile dataset locations, record lengths and depth. FR2 stands for IFREMER and PT for HIDROGRAFICO. ADCP working frequency is present in System column.

Project		Position (WGS-84)		System	Record length (days)	Depth (m)
ASPEX	FR2	44° 00′ N	001° 33′ W	ADCP 300 kHz	47	70
HERMIONE	PT	39° 48′ N	009° 12′ W	ADCP 300 kHz	46	80
MITIC	PT	38° 52′ N	009° 55′ W	ADCP 190 kHz	6	120
SIRIA	PT	37° 02′ N	007° 34′ W	ADCP 300 kHz	42	75

their own harmonic constants were used to validate present model results.

Four Acoustic Doppler Current Profiler (ADCP) records were validated and reprocessed to extract the barotropic tidal current. These datasets were obtained at depths of near 100 m, over different mid-shelf regions (Fig. 1). The ADCPs profiled the water column velocities from bottom to surface, enabling a vertical data integration to obtain the barotropic component of the observed current. These time series (Table 2) were submitted to similar harmonic analysis in order to calculate current ellipses for each tidal constituent.

2.2. Numerical model

The *HYbrid Coordinate Ocean Model* (HYCOM) is a hydrostatic primitive equations, free surface, ocean general circulation model (Bleck, 2002) that evolved from the *Miami Isopycnic-Coordinate Ocean Model*, MICOM (Bleck and Boudra, 1981; Bleck and Smith, 1990). The present work used the new HYCOM barotropic/baroclinic time-splitting scheme, recently modified to resolve external gravity waves over wet-and-dry regions (Morel et al., 2008). The model was also customized to force tidal solutions (sea-level and current velocity) as boundary conditions at the open frontiers. Gravitational tidal gradient force was added to HYCOM's momentum equations.

The model was used in 2D isopycnical single-layer configuration (pure barotropic mode), suitable for long-period gravity waves studies. This option has a smaller numerical cost and enables multiple one-year runs in a short period of time. By imposing the polychromatic tidal spectrum as the boundary condition, HYCOM radiates the correspondent waves by resolving both momentum (1) and continuity (2) equations, in the following adiabatic isopycnic forms. The single-layer nonlinear momentum equations (Bleck and Smith, 1990) are:

$$\begin{aligned}\frac{\partial u}{\partial t}+\frac{\partial}{\partial x}\frac{U^2}{2}-(\zeta+f)v&=-\frac{\partial M}{\partial x}+\frac{1}{H}[g\Delta\tau_{bx}+\nabla\cdot(\upsilon H\nabla u)]\\ \frac{\partial v}{\partial t}+\frac{\partial}{\partial y}\frac{U^2}{2}-(\zeta+f)u&=-\frac{\partial M}{\partial y}+\frac{1}{H}[g\Delta\tau_{by}+\nabla\cdot(\upsilon H\nabla v)]\end{aligned} \tag{1}$$

where u, v are the horizontal components of the velocity vector U, ζ is the relative vorticity, f the Coriolis parameter, $M=g\eta$ the Montgomery potential (g gravity, H the mean depth at rest and η the sea-surface elevation), $\Delta\tau_b$ the bottom stress gradient and υ is an horizontal turbulent viscosity coefficient. The general continuity equation, in single-layer configurations, is

$$\frac{\partial\eta}{\partial t}+\nabla\cdot((H+\eta)\cdot U)=0 \tag{2}$$

The bottom stress is formulated by a quadratic function of the barotropic current, parameterized by a drag coefficient, $\tau_b=-C_D|\,U\,|\,U$. For the present study, the momentum diffusion term is configured with a simple Smagorinsky frictional harmonic parameterization, where υ is defined as the maximum value of the following relation:

$$\upsilon=\max\left\{U_2dx;\quad\lambda_2\left[\left(\frac{\partial u}{\partial x}-\frac{\partial v}{\partial y}\right)^2+\left(\frac{\partial u}{\partial y}+\frac{\partial v}{\partial x}\right)^2\right]^{1/2}dx^2\right\} \tag{3}$$

where λ_2 is an eddy viscosity coefficient and U_2 is a diffusivity parameter. Spatial resolution was set to 1 arc-minute ARAWAKA-C grid ($dx=dy\sim1.8$ km).

2.2.1. Friction parameterization

Shallow water tides can physically create residual currents (tidal rectification), arising from the asymmetry between the flooding and ebbing phases (over very shallow water regions) or from local vorticity generation (especially near coastline and sloping topography). In nature, tidal rectification residual currents are usually one or two orders magnitude smaller than the forcing tidal flow velocities (Robinson, 1981). The use of discrete approximations to solve the momentum advection terms, in Eulerian equations, is also a source of artificial residual circulation. The resulting numerical diffusion is function of the grid resolution and the velocity shear. To minimize this effect, viscosity coefficients (3) were introduced to parameterize **turbulent friction** U_2 controls the numerical diffusion introduced by the unresolved scales within a constant grid resolution; λ_2 limits the uncontrolled turbulent diffusion added by strong velocity shears (verified over steep topography and rough coastlines). However, strong coefficients will falsely reduce the linear tidal velocity magnitude. This parameterization becomes then a compromise between an efficient numerical diffusion reduction and a realistic tide velocity simulation.

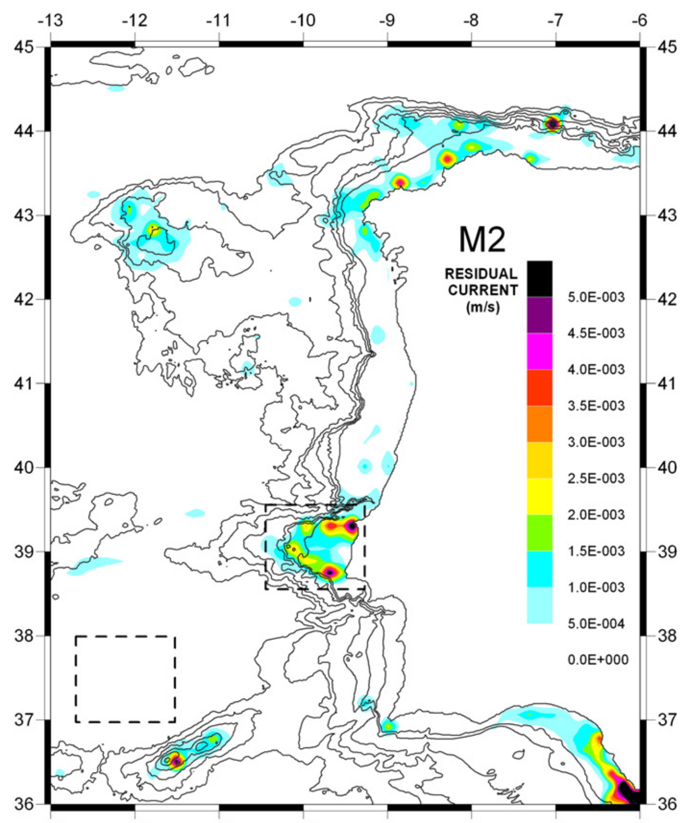

Fig. 3. M2 residual current extracted from harmonic analysis. Model parameterization: lateral friction enabled; $C_D=2.5\times10^{-3}$; $\lambda_2=0.2$ and $U_2=0.04$ m.s^{-1}. Two control areas are represented: 1. Offshore, where bottom topography is deep and flat, the numerical diffusion was reduced to values lower than 5×10^{-4} m.s^{-1}; inshore, over the Portuguese margin, the residual circulation arises at this region of strong slope and coastline roughness (reaching values $>5\times10^{-3}$ m.s^{-1}).

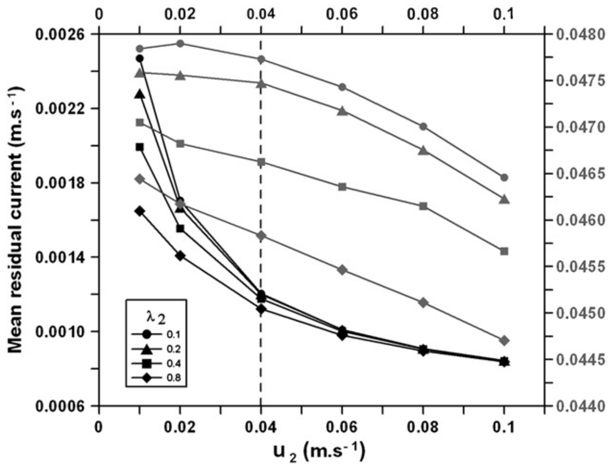

Fig. 4. Viscosity parameters evaluation. Several runs were performed with monochromatic tide (M2) and different viscosity parameterization. The residual current and M2 velocity amplitude was extracted from harmonic analysis and quantified at the control area 2, placed over the Portuguese shelf (see location at Fig. 3).

The adopted viscosity coefficients, λ_2 and U_2, were defined by optimal adjustment. Several monochromatic simulations were performed with different coefficient choices. The tidal current was extracted from each simulated solutions by harmonic analysis. A control sub-domain (see Fig. 3), covering the continental slope and shelf region, was chosen to quantify a mean coastal M2 velocity magnitude, as well as a mean residual current (non-harmonic circulation). The results were assembled with the variation range of the two viscosity coefficients (Fig. 4). Small λ_2 and U_2 values conduct to strong residual velocities and unvarying harmonic velocity magnitudes. On the other hand, strong λ_2 and U_2 values reduce the tidal velocity and converge the residual current to a minimum magnitude. In order to minimize the artificial residual flow and retain a steady tidal current magnitude the following parameter values were chosen: $\lambda_2 = 0.2$ and $U_2 = 0.04$ m.s^{-1}.

Boundary lateral friction was set to force a null tangential velocity at the coastline (no slip condition). Simulations with other boundary conditions reveal the intensification of artificial circulation along this frontier (not shown here). A standard drag coefficient of $C_D = 2.5 \times 10^{-3}$ was adopted to parameterize the bottom stress. In the present single layer configuration this parameter plays a small role, since water depth is high over most of the domain (Prandle, 1997). Simulations with other drag coefficient values (between 0.5×10^{-3} to 3.0×10^{-3}) gave no significant impact to the tidal solution (not shown here).

2.3. Bathymetry

The accuracy of regional tide models is often limited by bottom topography errors, normally manifested over the shelf and shallow regions. In recent years some global bathymetry datasets were made available, derived from both hydrographic soundings and the inversion of sea-surface satellite altimetry measurements. Over the study region, a common used bathymetry is the ETOPO1 global relief model (Amante and Eakins, 2009). However, this source reveals some inaccuracies over the Iberian shelf and misses topographic details along its continental slope. To overcome this problem, a new 1 arc-minute bathymetric Digital Terrain Model (DTM) of the West-Iberia domain was built from different bathymetry databases (called here after WIBM2009). Accurate data, detained by both Portuguese and French Hydrographic Offices (HIDROGRAFICO and SHOM) were complemented with ETOPO1 where no available hydrographic data existed.

WIBM2009 ensures a more realistic bathymetry over the Portuguese and Galicia region, where abrupt shelf discontinuities and complex coastline coexist in shallow-water regions. The domain extends from 32.0° to 46.0°N latitudes and from 16.0° to 1.0°W longitudes. It is horizontally referenced to the ellipsoid WGS-84 and vertically to the Portuguese hydrographic zero. For the present use, WIBM2009 was projected to MERCATOR coordinate system and vertically to the Mean Sea-Level by the use of MARMONDE MSL solution (Simon, 2007).

2.4. Tidal forcing

Tides are predominantly simulated in regional circulation numerical models by boundary conditions forcing. The sea-surface elevation and the corresponding 2D velocity components are imposed as tidal harmonics along the open limits. These ocean basin solutions are obtained from global ocean tide models, normally accurate in the deep-ocean but with significant errors near coastal and shallow regions. The present work explores the use of two recently revised and updated global tide solutions: TPXO7.2 and NEA2004 Tidal Atlas. Each results from different modelling approaches. TPXO7.2 is the most recent solution of the OTIS model (Egbert et al., 1994) that best fits the Laplace tidal equations to altimetry data from TOPEX/Poseidon plus Jason (since 2002 until present). The North-East Atlantic tidal atlas (NEA2004) results from a regional nesting of FES2004 (Lyard et al., 2006), carried out by the Toulouse Unstructured Grid Ocean model (T-UGOm) in a 2D barotropic, shallow water mode (Pairaud et al., 2008). FES2004 is also a global tide hydrodynamic model, improved by tide-gauge and altimetry data assimilation (TOPEX/Poseidon plus ERS-2).

The two global solutions were introduced, one at a time, as HYCOM's open boundary conditions. The performance of each simulation was evaluated by comparing harmonic analysis of the sea-surface height with the tide-gauge records network (Fig. 1). This accuracy assessment showed better semi-diurnal results when NEA2004 was applied and better diurnal solutions when TPXO7.2 was used. Exception was found in the K2 constituent. The adopted polychromatic solution, used as boundary conditions in the present HYCOM configuration, resulted from the assembling of N2, M2 and S2 constituents from NEA2004 and K2, Q1, O1, P1 and K1 from TPXO7.2. This choice allowed the best regional tide prediction and was made possible because, in the harmonic decomposition of the tide, the eight adopted constituents are independent from each other.

A further step was made to simulate the astronomical tide-raising forces acting regionally inside the study domain. The gravitational tidal gradient force, $\partial P/\partial x$ and $\partial P/\partial y$, was added to HYCOM barotropic momentum equations (1), as:

$$P = C_L \; g \sum_i \; \varphi_i \; a_i \; D_i \; \cos[q_i(t - t_0) + V_i(t_0) + b_i] \tag{4}$$

where C_L is the moon's reference potential (0.2687536×10^{-3} km), φ_i a Latitude coefficient, D_i the Doodson coefficient for each constituent (i) and a_i, b_i the respective nodal corrections parameters.

3. Model accuracy

The regional barotropic tide solution was obtained through one-year simulation, forced by polychromatic tidal spectrum (assembling four diurnal and four semi-diurnal constituents). The simulation started with an ocean at rest and the tide was introduced as boundary conditions with an exponential growth, completed after 10 semi-diurnal cycles. This option enabled the smooth settling of the tidal current inside the domain.

3.1. Sea surface height

Tidal sea-level amplitude and phase solutions were validated against harmonic analysis of tide gauge records, placed along the domain's coastline. La Coruña, Leixões, Peniche, Cascais, Sines and Lagos were chosen to represent the regional solution along the Portuguese and Galician West-coast (Section 4). Casablanca and Saint-Jean-de-Luz (Socoa) were chosen as representatives of the near open boundary tidal solution. All the other tide-gauges gave an overall model accuracy response. Model performance at the Gibraltar strait is not discussed here, since this is a complex domain where more careful work should be dedicated. However, this region was included in the model's domain since it modifies the tidal wave solution inside the gulf of Cadiz, which was validated by the Huelva tide-gauge.

The selected gauges were compared with their nearest grid point in the model. The eight tidal constituents were evaluated in amplitude and phase, expressed in Table 3 for semi-diurnal harmonics and Table 4 for diurnal. Confidence intervals were

Table 3
Accuracy evaluations of the model in the simulation of semi-diurnal tidal constituents. This estimation was made by the differences of the harmonics parameters (amplitude and phase) between tide-gauge records and model results (at the nearest point). The biggest differences were shaded. For each calculated value a confidence interval size was added (estimation error). In the model accuracy column the errors correspond to the sum of the previous two confidence intervals (tide-gauge plus model).

Harmonics		Tide gauge				Model				Model Accuracy					
name	period (hours)	amplitude		phase		amplitude		phase		amplitude			phase		
		(cm)	error (cm)	(°)	error (°)	(cm)	error (cm)	(°)	error (°)	(cm)	%	error (cm)	(°)	(min)	error (°)
SAINT JEAN–DE LUZ															
N2	12,658	28,12	0,36	73,31	0,76	28,11	< 0,01	70,47	0,01	0,00	0,01	0,37	2,84	5,99	0,77
M2	12,421	132,04	0,41	94,03	0,17	132,56	< 0,01	92,17	0,00	−0,52	−0,40	0,42	1,86	3,85	0,17
S2	12,000	45,96	0,43	126,34	0,51	44,81	< 0,01	124,14	0,01	1,15	2,50	0,44	2,20	4,40	0,52
K2	11,967	12,88	0,47	126,14	2,27	13,23	< 0,01	120,10	0,02	−0,35	−2,72	0,48	6,04	12,05	2,29
SANTANDER															
N2	12,658	28,20	–	76,25	–	27,55	<0,01	70,66	0,01	0,65	2,29	–	5,59	11,79	–
M2	12,421	134,29	–	95,43	–	129,97	<0,01	92,22	0,00	4,32	3,22	–	3,21	6,65	–
S2	12,000	46,56	–	128,71	–	43,91	<0,01	123,89	0,01	2,65	5,69	–	4,82	9,64	–
K2	11,967	13,08	–	126,89	–	12,96	<0,01	119,92	0,02	0,12	0,94	–	6,97	13,90	–
GIJON															
N2	12,658	27,52	–	71,45	–	26,98	<0,01	70,17	0,01	0,54	1,97	–	1,28	2,70	–
M2	12,421	131,08	–	91,20	–	127,29	<0,01	91,59	0,00	3,79	2,89	–	−0,39	−0,81	–
S2	12,000	45,83	–	123,43	–	43,02	<0,01	122,90	0,01	2,81	6,14	–	0,53	1,06	–
K2	11,967	13,11	–	121,41	–	12,68	<0,01	119,01	0,02	0,43	3,30	–	2,40	4,79	–
CORUNHA–2															
N2	12,658	25,42	–	67,73	–	25,08	<0,01	66,14	0,01	0,34	1,34	–	1,59	3,35	–
M2	12,421	120,18	–	86,68	–	118,03	<0,01	87,05	0,00	2,15	1,79	–	−0,37	−0,77	–
S2	12,000	42,19	–	117,97	–	39,98	<0,01	117,34	0,01	2,21	5,24	–	0,63	1,26	–
K2	11,967	11,81	–	115,67	–	11,70	<0,01	113,58	0,02	0,11	0,94	–	2,09	4,17	–
LEIXOES															
N2	12,658	22,26	0,16	58,55	0,40	22,55	<0,01	55,64	0,01	−0,28	−1,28	0,17	2,91	6,14	0,41
M2	12,421	104,65	0,17	76,42	0,09	105,03	<0,01	75,21	0,00	−0,37	−0,36	0,18	1,21	2,50	0,09
S2	12,000	36,44	0,16	104,66	0,25	35,76	<0,01	103,17	0,01	0,67	1,85	0,17	1,49	2,98	0,26
K2	11,967	10,23	0,11	101,69	0,65	10,34	<0,01	100,61	0,02	−0,11	−1,08	0,12	1,08	2,15	0,67
PENICHE															
N2	12,658	21,94	0,15	51,57	0,44	22,13	0,01	51,30	0,01	−0,18	−0,83	0,16	0,27	0,57	0,45
M2	12,421	102,95	0,16	69,62	0,09	102,89	0,01	70,21	0,00	0,06	0,06	0,17	−0,59	−1,22	0,09
S2	12,000	35,77	0,14	96,99	0,27	35,17	0,01	97,15	0,01	0,60	1,68	0,15	−0,16	−0,32	0,28
K2	11,967	9,93	0,12	93,83	0,59	10,11	0,01	94,99	0,01	−0,18	−1,77	0,13	−1,16	−2,31	0,60
CASCAIS															
N2	12,658	21,20	0,13	46,95	0,34	21,36	0,01	46,90	0,01	−0,16	−0,75	0,14	0,05	0,11	0,35
M2	12,421	99,18	0,14	64,11	0,08	99,12	0,01	65,22	0,00	0,06	0,06	0,15	−1,11	−2,30	0,08
S2	12,000	34,91	0,13	90,71	0,22	34,08	0,01	90,54	0,00	0,83	2,38	0,14	0,17	0,34	0,22
K2	11,967	9,73	0,10	86,90	0,54	9,73	0,01	89,54	0,01	0,00	−0,01	0,11	−2,64	−5,27	0,55
SINES															
N2	12,658	21,33	0,17	46,58	0,52	21,53	<0,01	45,73	0,01	−0,20	−0,94	0,18	0,85	1,79	0,53
M2	12,421	99,21	0,15	63,61	0,10	99,88	<0,01	63,90	0,00	−0,67	−0,68	0,16	−0,29	−0,60	0,10
S2	12,000	34,90	0,18	90,15	0,28	34,34	<0,01	89,85	0,00	0,56	1,60	0,19	0,30	0,60	0,28
K2	11,967	9,52	0,13	86,91	0,79	9,79	<0,01	88,07	0,01	−0,27	−2,81	0,14	−1,16	−2,31	0,80
LAGOS															
N2	12,658	21,11	0,15	41,21	0,38	21,65	<0,01	41,57	0,00	−0,54	−2,54	0,16	−0,36	−0,76	0,38
M2	12,421	99,09	0,13	57,68	0,09	100,50	<0,01	59,16	0,00	−1,42	−1,43	0,14	−1,48	−3,06	0,09
S2	12,000	35,68	0,14	83,04	0,21	34,87	<0,01	84,49	0,00	0,82	2,29	0,15	−1,45	−2,90	0,21
K2	11,967	9,88	0,11	79,47	0,62	9,85	<0,01	82,60	0,01	0,03	0,27	0,12	−3,13	−6,24	0,63
HUELVA–5															
N2	12,658	22,51	–	41,83	–	22,33	<0,01	40,06	0,01	0,18	0,80	–	1,77	3,73	–
M2	12,421	104,97	–	57,99	–	103,58	<0,01	57,58	0,00	1,39	1,32	–	0,41	0,85	–
S2	12,000	38,47	–	85,16	–	35,88	<0,01	83,00	0,00	2,59	6,72	–	2,16	4,32	–
K2	11,967	10,76	–	83,01	–	10,10	<0,01	80,40	0,01	0,66	6,09	–	2,61	5,21	–
CASABLANCA															
N2	12,658	20,86	1,11	37,92	3,24	22,12	<0,01	37,74	0,00	1,26	6,02	1,12	−0,18	−0,38	3,24
M2	12,421	98,99	1,08	55,86	0,73	102,43	<0,01	54,84	0,00	3,44	3,47	1,09	−1,02	−2,11	0,73
S2	12,000	35,39	1,27	80,84	1,94	35,50	<0,01	79,48	0,00	0,11	0,30	1,28	−1,36	−2,72	1,94
K2	11,967	9,75	1,67	76,52	9,14	9,94	<0,01	78,25	0,01	0,19	1,91	1,68	1,73	3,45	9,15

added to the harmonic parameters estimation (amplitude and phase), function of each record lengths and time-series noise (from Pawlowicz et al., 2002). The model accuracy was expressed by the differences between the simulated and the observed tide, at each tide-gauge location. It is important to point out that the interpretation of these differences should take into account the related confidence intervals.

The model revealed a very good performance, especially in the semi-diurnal constituents. Generally, each semi-diurnal harmonic was reproduced with amplitude errors lower than 1 cm (corresponding to an amplitude percentage lower than 3%) and phase mismatch shorter than 5 min (equivalent to less than 2.5°). Exception must be pointed out to the S2 constituent, with a slightly higher amplitude error over the Spanish coast, ~2.5 cm (equivalent to 6%). The fact

Table 4
Accuracy evaluations of the model in the simulation of diurnal tidal constituents. This estimation was made by the differences of the harmonics parameters (amplitude and phase) between tide-gauge records and model results (at the nearest point). The biggest differences were shaded. For each calculated value a confidence interval size was added (estimation error). In the model accuracy column the errors correspond to the sum of the previous two confidence intervals (tide-gauge plus model).

Harmonics		Tide gauge				Model				Model Accuracy					
name	period (hours)	amplitude		phase		amplitude		phase		amplitude			phase		
		(cm)	error (cm)	(°)	error (°)	(cm)	error (cm)	(°)	error (°)	(cm)	%	error (cm)	(°)	(min)	error (°)
SAINT JEAN–DE LUZ															
Q1	26,867	2,27	0,11	267,27	2,99	2,36	< 0,01	269,19	0,07	−0,09	−3,97	0,12	−1,92	−8,60	3,06
O1	25,820	7,02	0,11	318,97	0,95	7,40	< 0,01	314,81	0,02	−0,38	−5,34	0,12	4,16	17,90	0,97
P1	24,067	1,93	0,12	54,84	2,78	1,69	< 0,01	59,77	0,11	0,24	12,32	0,13	−4,93	−19,78	2,89
K1	23,935	6,19	0,11	69,49	1,13	5,73	< 0,01	67,97	0,03	0,46	7,43	0,12	1,52	6,06	1,16
SANTANDER															
Q1	26,867	2,24	–	277,08	–	2,28	<0,01	268,99	0,07	−0,04	−1,76	–	8,09	36,23	–
O1	25,820	7,15	–	324,02	–	7,10	<0,01	316,69	0,02	0,05	0,66	–	7,33	31,54	–
P1	24,067	2,04	–	59,06	–	1,82	<0,01	62,42	0,11	0,22	10,71	–	−3,36	−13,48	–
K1	23,935	6,60	–	71,49	–	6,16	<0,01	69,86	0,03	0,44	6,70	–	1,63	6,50	–
GIJON															
Q1	26,867	2,10	–	280,00	–	2,21	<0,01	268,56	0,08	−0,11	−5,11	–	11,44	51,23	–
O1	25,820	7,03	–	323,96	–	6,83	<0,01	318,46	0,02	0,20	2,86	–	5,50	23,67	–
P1	24,067	2,24	–	59,22	–	1,93	<0,01	64,51	0,10	0,31	13,82	–	−5,29	−21,22	–
K1	23,935	6,83	–	70,69	–	6,52	<0,01	71,40	0,02	0,31	4,59	–	−0,71	−2,83	–
CORUNHA–2															
Q1	26,867	2,18	–	271,19	–	2,06	<0,01	266,21	0,07	0,12	5,53	–	4,98	22,30	–
O1	25,820	6,77	–	324,74	–	6,37	<0,01	319,84	0,02	0,40	5,84	–	4,90	21,09	–
P1	24,067	2,38	–	60,77	–	2,12	<0,01	64,36	0,08	0,26	11,12	–	−3,59	−14,40	–
K1	23,935	7,67	–	73,21	–	7,18	<0,01	70,95	0,02	0,49	6,39	–	2,26	9,02	–
LEIXOES															
Q1	26,867	1,95	0,11	274,73	3,18	1,96	<0,01	262,93	0,07	−0,01	−0,47	0,12	11,80	52,84	3,25
O1	25,820	6,18	0,11	318,15	1,03	6,10	<0,01	316,98	0,02	0,08	1,27	0,12	1,17	5,03	1,05
P1	24,067	2,08	0,14	49,85	3,97	1,99	<0,01	56,58	0,09	0,08	3,98	0,15	−6,73	−27,00	4,06
K1	23,935	6,86	0,12	60,71	0,98	6,83	<0,01	62,36	0,02	0,02	0,36	0,13	−1,65	−6,58	1,00
PENICHE															
Q1	26,867	1,84	0,08	269,35	3,16	1,94	<0,01	257,45	0,07	−0,10	−5,40	0,09	11,90	53,29	3,23
O1	25,820	6,21	0,10	314,47	0,91	6,29	<0,01	314,44	0,02	−0,07	−1,20	0,11	0,03	0,13	0,93
P1	24,067	2,35	0,11	47,23	2,66	2,18	<0,01	57,53	0,08	0,17	7,06	0,12	−10,30	−41,32	2,74
K1	23,935	7,49	0,09	55,56	0,76	7,42	<0,01	62,92	0,02	0,08	1,01	0,10	−7,36	−29,36	0,78
CASCAIS															
Q1	26,867	2,06	0,06	262,30	1,71	1,87	<0,01	258,33	0,08	0,19	9,22	0,07	3,97	17,78	1,79
O1	25,820	5,93	0,06	314,84	0,61	5,93	<0,01	312,95	0,02	−0,01	−0,11	0,07	1,89	8,13	0,63
P1	24,067	2,16	0,08	44,03	2,07	1,97	<0,01	52,93	0,08	0,20	9,06	0,09	−8,90	−35,70	2,15
K1	23,935	6,93	0,06	54,13	0,51	6,75	<0,01	58,44	0,02	0,18	2,55	0,07	−4,31	−17,19	0,53
SINES															
Q1	26,867	1,95	0,06	265,81	1,85	1,89	<0,01	257,60	0,08	0,06	3,09	0,07	8,21	36,76	1,93
O1	25,820	6,05	0,07	314,39	0,54	6,02	<0,01	311,51	0,02	0,03	0,42	0,08	2,88	12,39	0,56
P1	24,067	2,19	0,07	45,08	1,81	1,96	<0,01	51,98	0,08	0,23	10,28	0,08	−6,90	−27,68	1,89
K1	23,935	6,85	0,07	55,14	0,52	6,75	<0,01	57,57	0,02	0,10	1,47	0,08	−2,43	−9,69	0,54
LAGOS															
Q1	26,867	1,96	0,07	252,21	2,34	1,84	<0,01	255,29	0,08	0,12	6,12	0,08	−3,08	−13,79	2,42
O1	25,820	5,93	0,08	309,56	0,78	5,95	<0,01	308,11	0,02	−0,01	−0,21	0,09	1,45	6,24	0,80
P1	24,067	2,24	0,10	40,56	2,23	1,89	<0,01	47,55	0,08	0,35	15,73	0,11	−6,99	−28,04	2,31
K1	23,935	6,71	0,08	48,92	0,71	6,50	<0,01	53,26	0,02	0,21	3,14	0,09	−4,34	−17,31	0,73
HUELVA–5															
Q1	26,867	1,83	–	265,12	–	1,86	<0,01	256,17	0,11	−0,03	−1,90	–	8,95	40,08	–
O1	25,820	6,12	–	311,52	–	6,12	<0,01	305,52	0,03	0,00	−0,02	–	6,00	25,82	–
P1	24,067	2,51	–	42,28	–	1,73	<0,01	43,61	0,11	0,78	31,20	–	−1,33	−5,33	–
K1	23,935	6,81	–	50,38	–	5,98	<0,01	49,66	0,04	0,83	12,15	–	0,72	2,87	–
CASABLANCA															
Q1	26,867	1,70	0,28	253,43	9,03	1,95	<0,01	252,92	0,07	0,25	14,94	0,29	−0,51	−2,28	9,10
O1	25,820	5,83	0,33	309,93	2,55	6,05	<0,01	305,34	0,02	0,22	3,79	0,34	−4,59	−19,75	2,57
P1	24,067	2,04	0,23	38,72	7,24	1,83	<0,01	48,53	0,09	−0,21	−10,38	0,24	9,81	39,35	7,33
K1	23,935	6,76	0,26	48,15	2,16	6,30	<0,01	54,41	0,02	−0,46	−6,82	0,27	6,26	24,97	2,18

that both Casablanca and Saint Jean-de-Luz evidenced lower S2 mismatch reflects a probable discrepancy in the adopted harmonic analysis methods (between the one used in the present work and the method used by Puertos del Estado) or a sensitive result to less accurate bathymetry data detained by WIBM2009 over the Northern Spanish continental margin (Section 2.3).

The model was less accurate in the simulation of the diurnal constituents. Amplitudes were reproduced with errors lower than 0.5 cm (corresponding to amplitude percentage lower than ~10%). However, phase discrepancies exceeded 30 min in some cases (corresponding to phase differences > 7°). These mismatches were higher near the open boundaries and reflect tide solutions inaccuracies transposed from the adopted Global models (Section 2.4). Nevertheless, the obtained accuracy was globally superior to previous literature results. This gave credit to the bathymetry improvement and to the polychromatic tidal forcing option.

3.2. Tidal currents

Four shallow water current profile measurements were used to validate the barotropic tidal velocities simulated by the model (Table 2). *In situ* and numerical time-series were evaluated by harmonic analysis. The resulting current velocity ellipses were compared for the major tidal constituents (Figs. 5, 6 and 7). The short ADCP record lengths (under 40 days) restricted this evaluation to the following semi-diurnal harmonics: M2, S2 and N2. The diurnal tidal ellipses are very small, of the order of a few millimetres per second. These values are near the threshold precision of the ADCP measurement and smaller than the adopted accuracy of the model (1 cm.s^{-1}). Exception was made to the MITIC record, where the diurnal velocity is magnified over the Tagus Plateau. However, the short record length and the high noise level disabled a precise evaluation of the K1 ellipse. For these reasons, diurnal ellipses were not evaluated.

The M2 current velocity was reproduced highly accurate over the shelf, generally matching the semi-major and semi-minor axis magnitude, orientation, phase and sense of rotation of the ellipses (Fig. 6). The small differences in the shape of each ellipse can be attributed to missing topographic detail within the 1-arc minute model resolution, as discussed next.

The HERMIONE simulated M2 ellipse differed only in the semi-minor axis magnitude and consequently shows higher eccentricity than the *in situ* observation. This is a direct consequence of the adopted model resolution, which transforms the narrow Nazaré canyon head into a deep channel that funnels the local tidal circulation.

The MITIC simulation reproduced the increase of the M2 current velocity magnitude, as well as the clockwise rotation sense, induced by the Tagus plateau configuration. However, a small difference exists in the ellipse orientation and phase. These two mismatches are linked and put in evidence a similar lack in topographic detail. This deduction comes from the existing correlation between the ellipse orientation, β, and the velocity phase, G, by $\beta = G + atan\ (i_p/r_p)$, where i_p and r_p are the trigonometric coefficients obtained by harmonic analysis.

ASPEX and SIRIA simulations highlighted the effective performance of the model in the reproduction of M2 tidal flow. Both model and observed ellipses match, with axis length error <5%, orientation error <5° and phase error <10° (Fig. 5).

Model results also showed a fair reproduction of S2 and N2 tidal current velocity constituents (Figs. 6 and 7). Here, the model performance was difficult to evaluate since these velocities are very small (~1 cm.s^{-1}). The critical parameter is the ellipse's eccentricity,

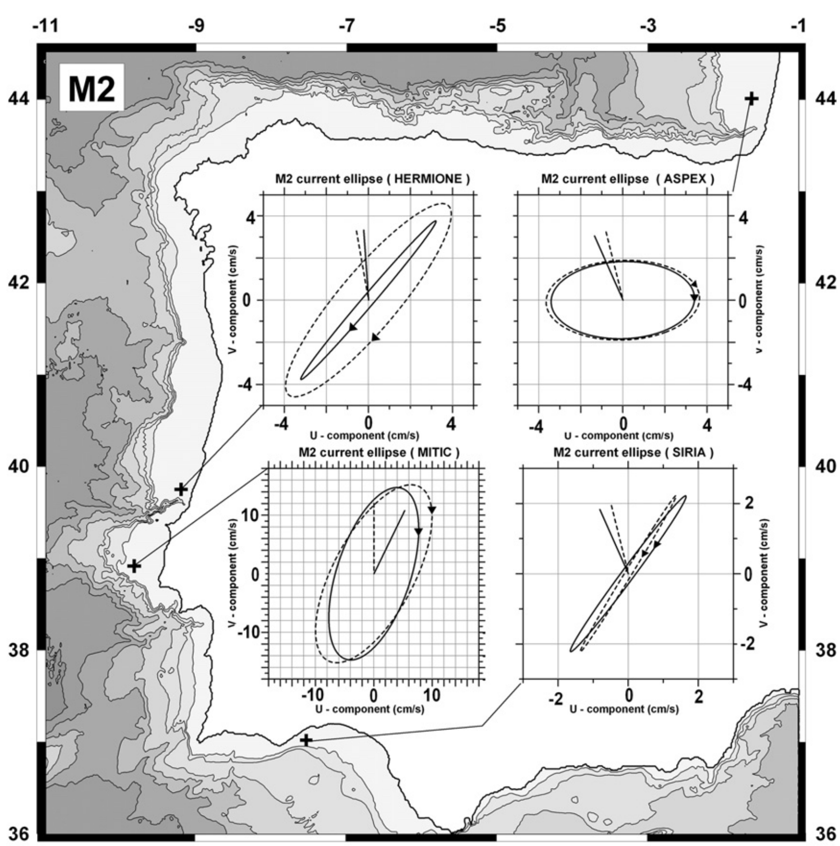

Fig. 5. Validation of the M2 tidal current simulated by the model. The tidal ellipses were obtained from ADCP datasets (dashed line) are compared with model results (solid line). The velocity phase is represented by the vector orientation (in polar coordinates) and the sense of rotation by the arrow.

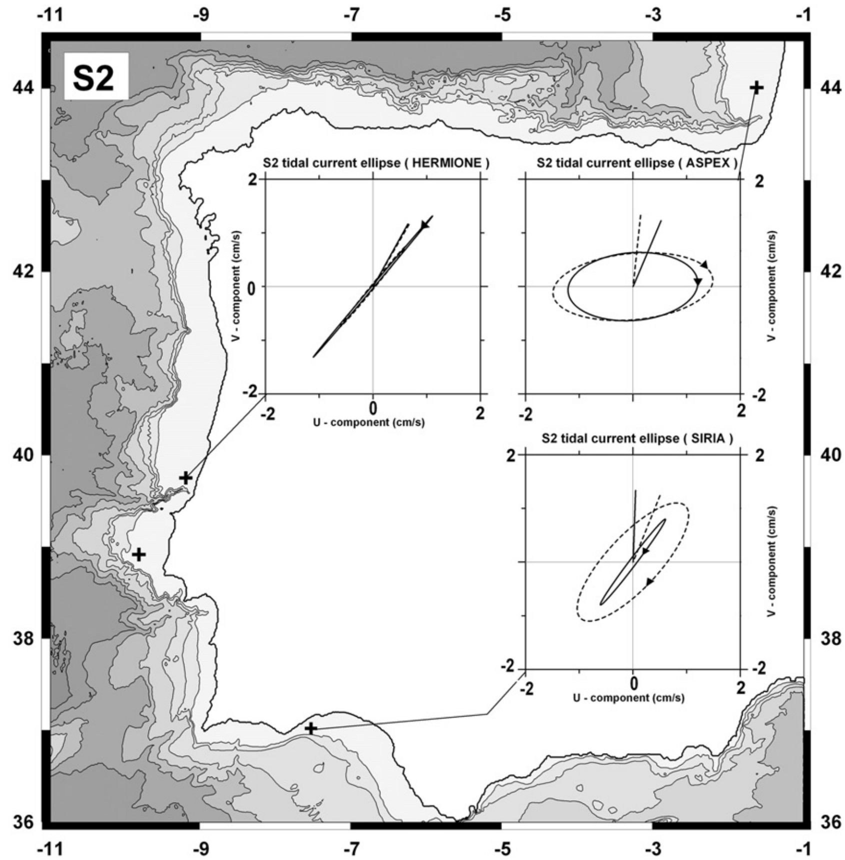

Fig. 6. Validation of the S2 tidal current simulated by the model. The tidal ellipses were obtained from ADCP datasets (dashed line) are compared with model results (solid line). The velocity phase is represented by the vector orientation (in polar coordinates) and the sense of rotation by the arrow. The short MITIC's time-series (~6 days) disables the estimation of the S2 constituent.

which is very sensitive to small-scale topographic details (hidden within the present model resolution).

4. Results

The accuracy of the model reveals a successful simulation of the barotropic tide, along the West-Iberian continental margin. The harmonic analysis of one-years simulation was assembled to construct tidal maps around the domain. The solution is hereafter evaluated by spatial analyses of the sea-surface height and barotropic tidal flow.

The tide shows a dual behaviour, distinct between semidiurnal and diurnal harmonics. This contrast is a function of the local inertial period $T_f = 2\pi/f$, that varies from ~17 h (45° N) to ~20.5 h (36° N) and divides the polychromatic tidal spectrum into a super-inertial (semi-diurnal constituents) and a sub-inertial group (diurnal constituents). N2, M2, S2 and K2 exhibit similar sea-surface amplitude and flow variability, differing from each other primarily in magnitude and phase values. In an analogous way, Q1, O1, P1 and K1 share the same intra-group behaviour, with different magnitude and phase values. From this, M2 and K1 were chosen to illustrate the distinct super-inertial and sub-inertial spatial structures. A zoom was made over the West-Iberian margin, from 36° to 45° N and from 6° to 13° W (study region).

4.1. Semidiurnal tide

Along the West-Iberian coast, the M2 is the most energetic tidal constituent, with sea surface amplitude (η ~1.0 m) and phase increasing from south to north (Fig. 8). Across-shelf, the amplitude decreases offshore with a mean gradient of ~0.027 cm.km^{-1}. Co-tidal lines are almost perpendicular to the coast, skirting regularly the continental margin, with a mean phase velocity of C_{M2} ~245 m.s^{-1} (calculated from numerical solution, between Cape of Sagres, 37° N, and Cape of Finisterra, 43° N). Offshore, the M2 velocity component perpendicular to the coast is almost inexistent and the ellipses are extremely eccentric, aligned tangentially to the West-Iberian margin (Fig. 10). These characteristics suggest a semi-diurnal tidal wave trapped as a Kelvin mode around the narrow West-Iberian shelf. This foremost tidal constituent is followed, with the same behaviour and spatial structure, by S2 (η ~ 0.35 m), N2 (η ~0.22 m) and K2 (η ~0.10 m).

The shelf width is determinant in the tidal wave amplitude and current velocity magnitude (Battisti and Clarke, 1982). For example, the M2 amplitude is smaller in the southern region (η <1 m), revealing locally the almost absent shelf. On the other hand, M2 is amplified along the wider northern Portuguese margin (η >1 m), especially over the Tagus plateau (η ~1.03 m) where the shelf reaches its maximum width (65 km).

The Bay of Biscay confines the tidal wave, forcing the amplification of the semi-diurnal constituents towards the French Armorican shelf. This semi-enclosed sea effect generates a strong amplitude gradient along the North-Iberian margin and especially at the Galician shelf (varying from η ~1.05 m at Leixões to η ~1.30 m at Gijon). A similar effect, in smaller proportions, is observed inside the Gulf of Cadiz (η ~1.05 m).

Over the slope and shelf, where the tidal phase velocity is not in balance with the varying depth, the Kelvin semi-geostrophic equilibrium breaks apart and the cross-shelf velocity component appears. This gives rise to rotary tidal currents in cyclonic sense. The ellipse eccentricity decreases as function of the shelf slope (Fig. 9).

Along-shelf, the semi-diurnal velocities show higher spatial variability than sea-surface amplitudes. The current is magnified (Fig. 10) and changes the rotation sense to anti-cyclonic (Fig. 9), over the major shelf-width anomalies (as submarine canyons and

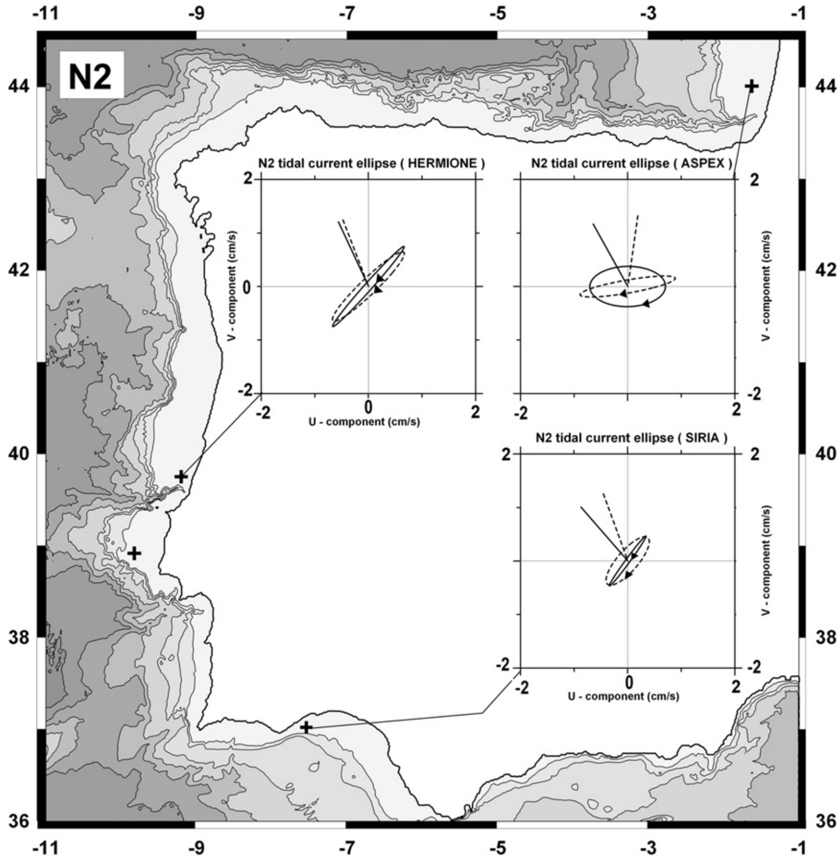

Fig. 7. Validation of the N2 tidal current simulated by the model. The tidal ellipses were obtained from ADCP datasets (dashed line) are compared with model results (solid line). The velocity phase is represented by the vector orientation (in polar coordinates) and the sense of rotation by the arrow. The short MITIC's time-series (~6 days) disables the estimation of the S2 constituent.

promontories). The same behaviour is observed around important Capes as Finisterra and Sagres, as well as over the nearby seamounts (Gorringe and Galicia banks). This effect seems to be linked to the fluid vorticity production over the strong along-shelf slopes that surround these topographic features.

4.2. Diurnal tide

The principal diurnal constituents are less energetic than the semi-diurnal. Nevertheless, they contribute significantly to the modulation of the tide along the domain (mainly forced by O1 and K1). The amplitude ratio between the semi-diurnal and diurnal group is smaller here than in nearby coastal regions, like in the Bay of Biscay (LeCann, 1990) or in the Gulf of Cadiz. The diurnal tidal amplitude grows from south to north, with maximums located at the Galician shelf and over the Tagus plateau (reaching $\eta = 7.4$ cm for K1). Its phase speed is locally lower than for the semi-diurnal tide (C_{K1} ~ 198 m.s^{-1}). Another important difference is the distortion of the diurnal cotidal lines, especially over the Portuguese shelf (Fig. 12). This fact results from the settling of continental shelf waves, trapped along the northern Portuguese coast. Their patterns are visible in K1 amplitudes (Fig. 12) and in current velocity phases (Fig. 15). This process is discussed in Section 5.

Diurnal tidal velocities are almost inexistent offshore (Fig. 13). They become measurable over the shelf and, like for the semi-diurnal constituents, are magnified over the major shelf width anomalies, capes and seamounts (Fig. 14). The diurnal ellipses are anti-cyclonic, as consequence of the sub-inertial forcing. The Q1, O1, P1 current velocities evidence similar spatial distribution as K1, different in magnitude but following the same ratio as presented in Fig. 2.

5. Analysis

Model results highlight complex tidal structures along the West-Iberian margin (Figs. 9–16). The large-scale tidal wave (propagating mainly in a Kelvin mode) runs along a narrow continental shelf, where the non-uniform depth gives rise to a wide set of possible coastal trapped modes (Huthnance, 1975). These modes are discrete solutions of the momentum and continuity equations, obtained in the frequency/wave number space [ω, k]. The trapping condition is defined by Eq. (5) and is translated by an offshore decay of the wave amplitude,

$$\omega/f < \sqrt{1 + gHk^2 f^{-2}} \tag{5}$$

For tidal forcing modes, the frequencies are fixed (harmonic constituents) and the wave number solutions, k, (or wavelengths by $\lambda = 2\pi/k$) are obtained as eigenvalues of the corresponding wave dispersion relationships (cross-shelf profile dependent).

The wave trapping is naturally ruled by the inertial frequency, f. This physical limit splits the full set of possible wave modes in two distinct domains: 1. Sub-inertial modes governed by the potential-vorticity conservation restoring force (continental shelf waves) and 2. Super-inertial modes governed mainly by gravity (edge waves). The Kelvin mode makes the exception, coexisting in both frequency domains ($0<\omega<\infty$) and simultaneously verifying the trapping condition. This fundamental solution is obtained by imposing a flat ocean bottom, bounded by a straight wall. As a result, the dispersion relationship, $\omega^2 = gHk^2$ (6), is independent of f and the wave gets a linear solution in the space [ω, k], simply function of a constant depth.

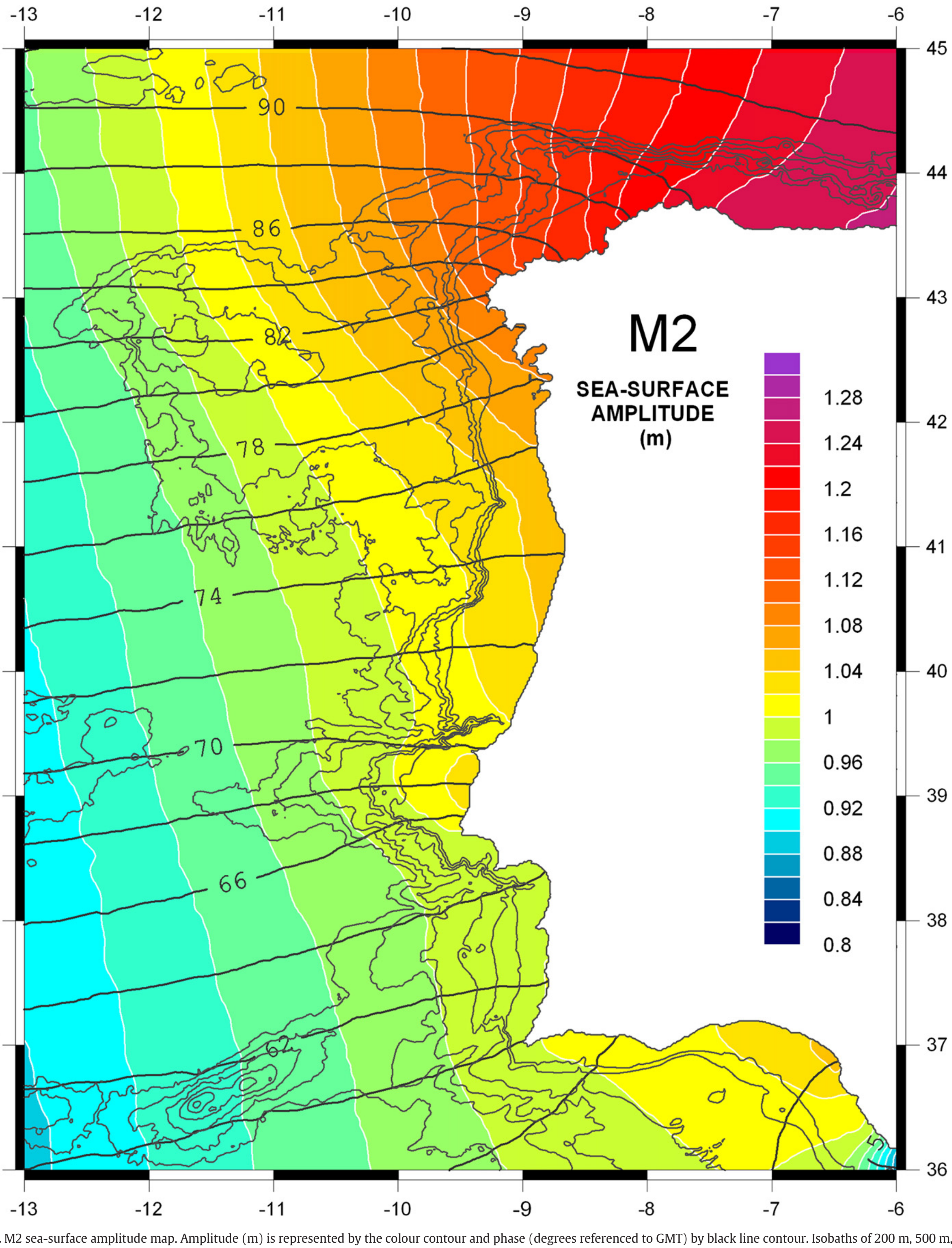

Fig. 8. M2 sea-surface amplitude map. Amplitude (m) is represented by the colour contour and phase (degrees referenced to GMT) by black line contour. Isobaths of 200 m, 500 m, 1000 m, 2000 m, 3000 m and 4000 m were added to help interpretation.

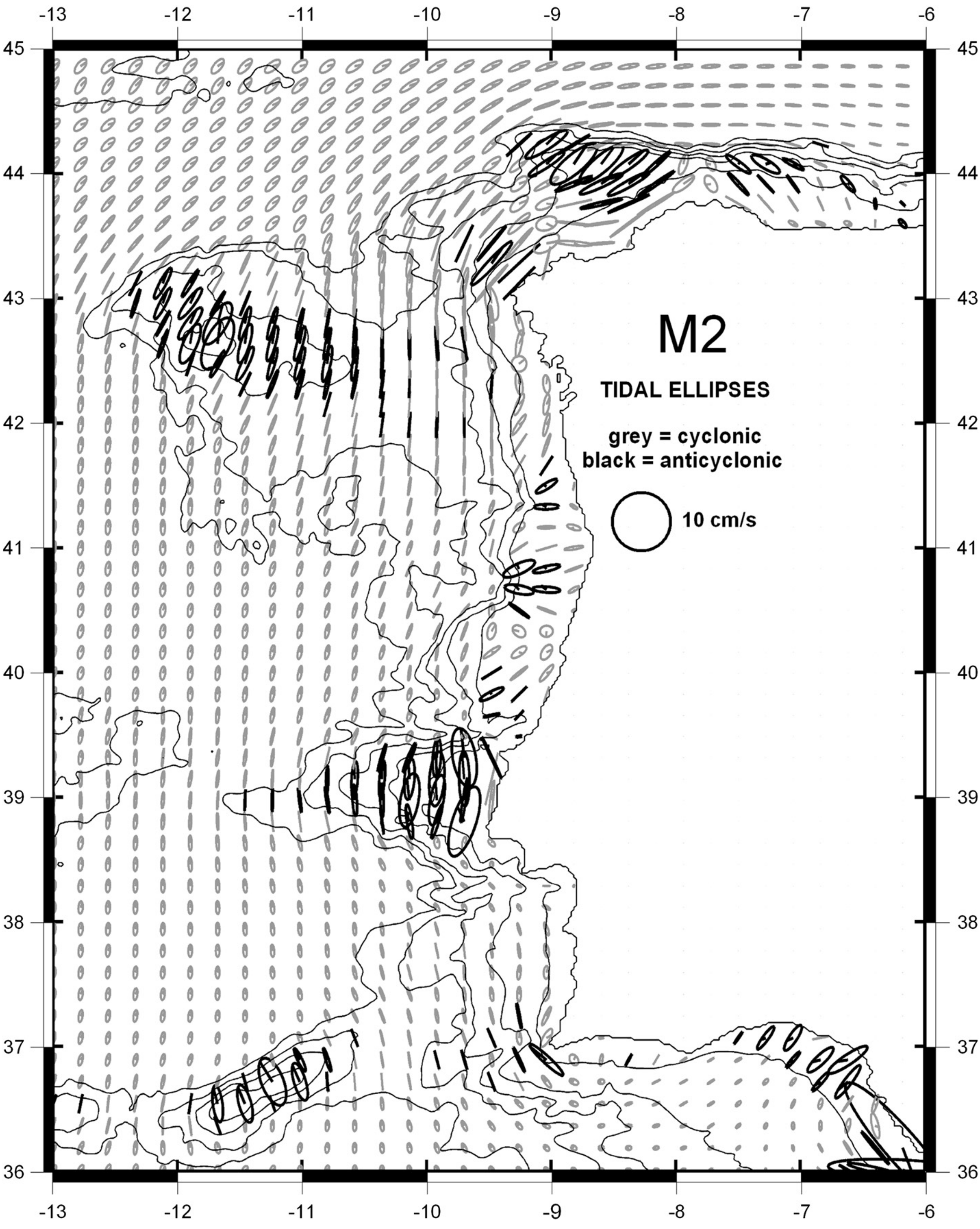

Fig. 9. M2 tidal ellipses map. The grey ellipses represent cyclonic rotation and the bold ellipses anti-cyclonic. The polar axis, traced inside each ellipse, represents the velocity phase and translates the M2 velocity vector at the same instance. Isobaths of 200 m, 500 m, 1000 m, 2000 m, 3000 m and 4000 m were added to help interpretation.

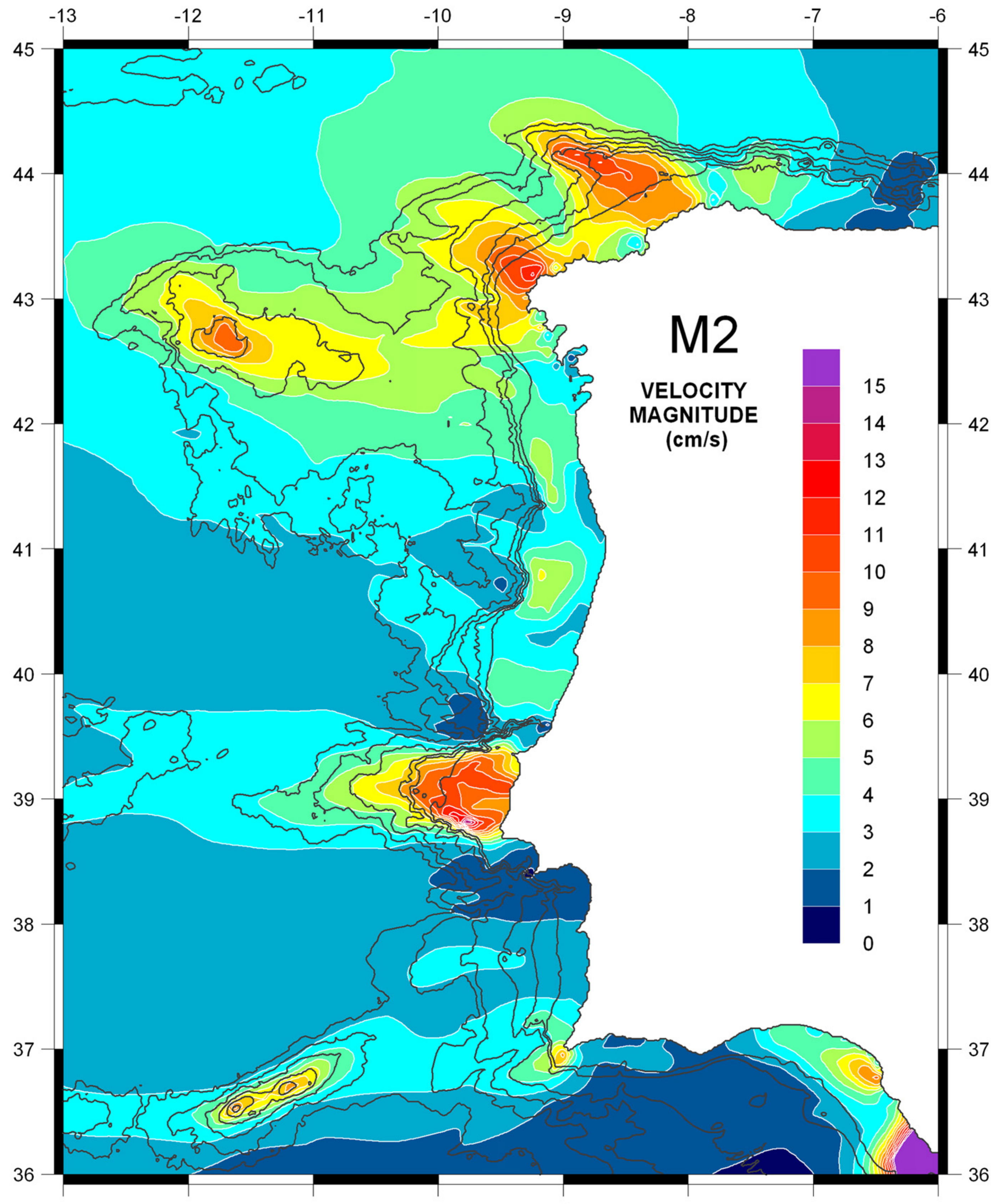

Fig. 10. M2 barotropic current velocity map. The maximum M2 velocities (cm.s^{-1}) are illustrated by the tidal ellipse semi-major axis magnitude. Isobaths of 200 m, 500 m, 1000 m, 2000 m, 3000 m and 4000 m were added to help interpretation.

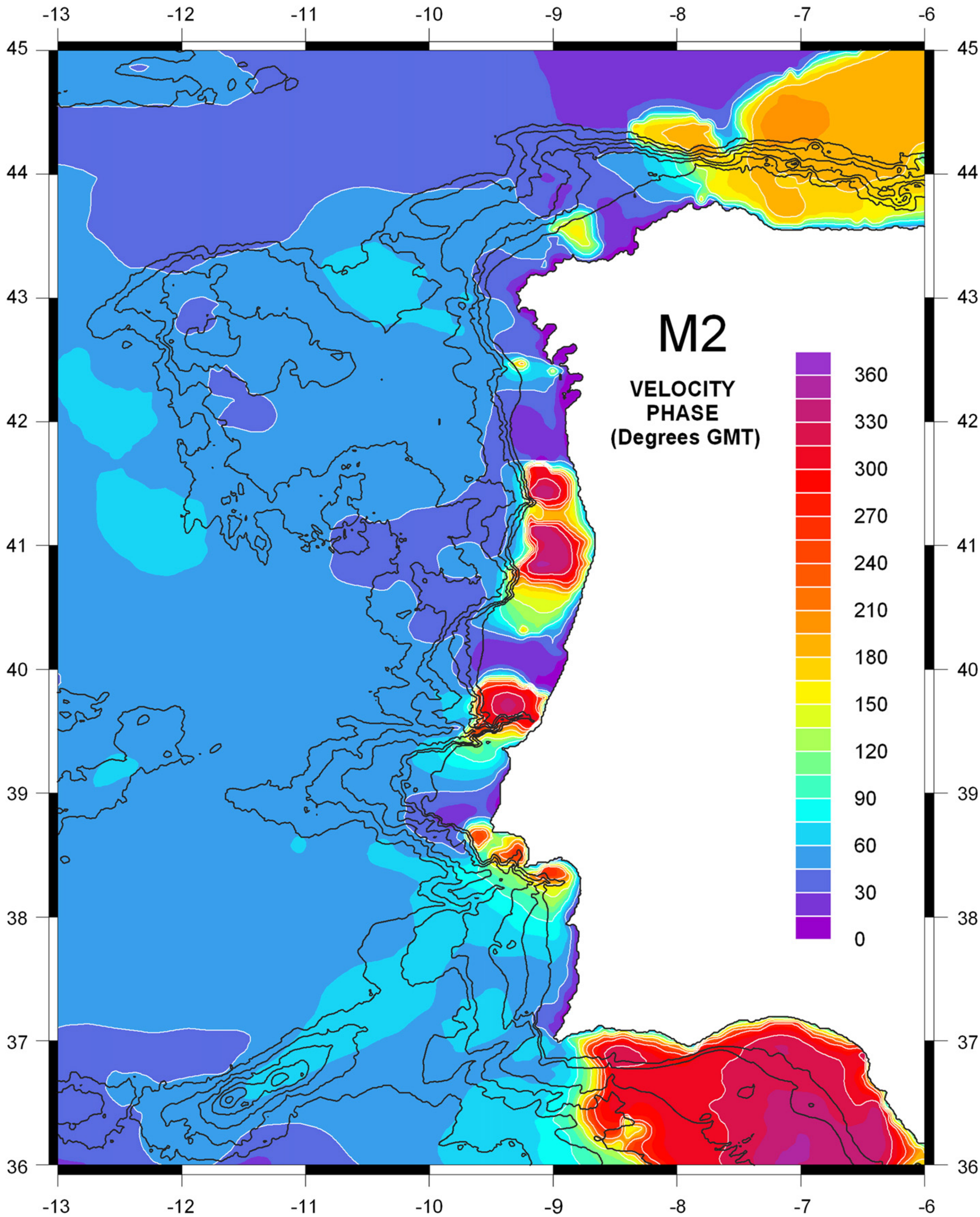

Fig. 11. M2 barotropic current velocity phase map. This corresponds to the phase lag of the maximum current behind the maximum tidal potential of M2 (degrees referenced to GMT). Isobaths of 200 m, 500 m, 1000 m, 2000 m, 3000 m and 4000 m were added to help interpretation.

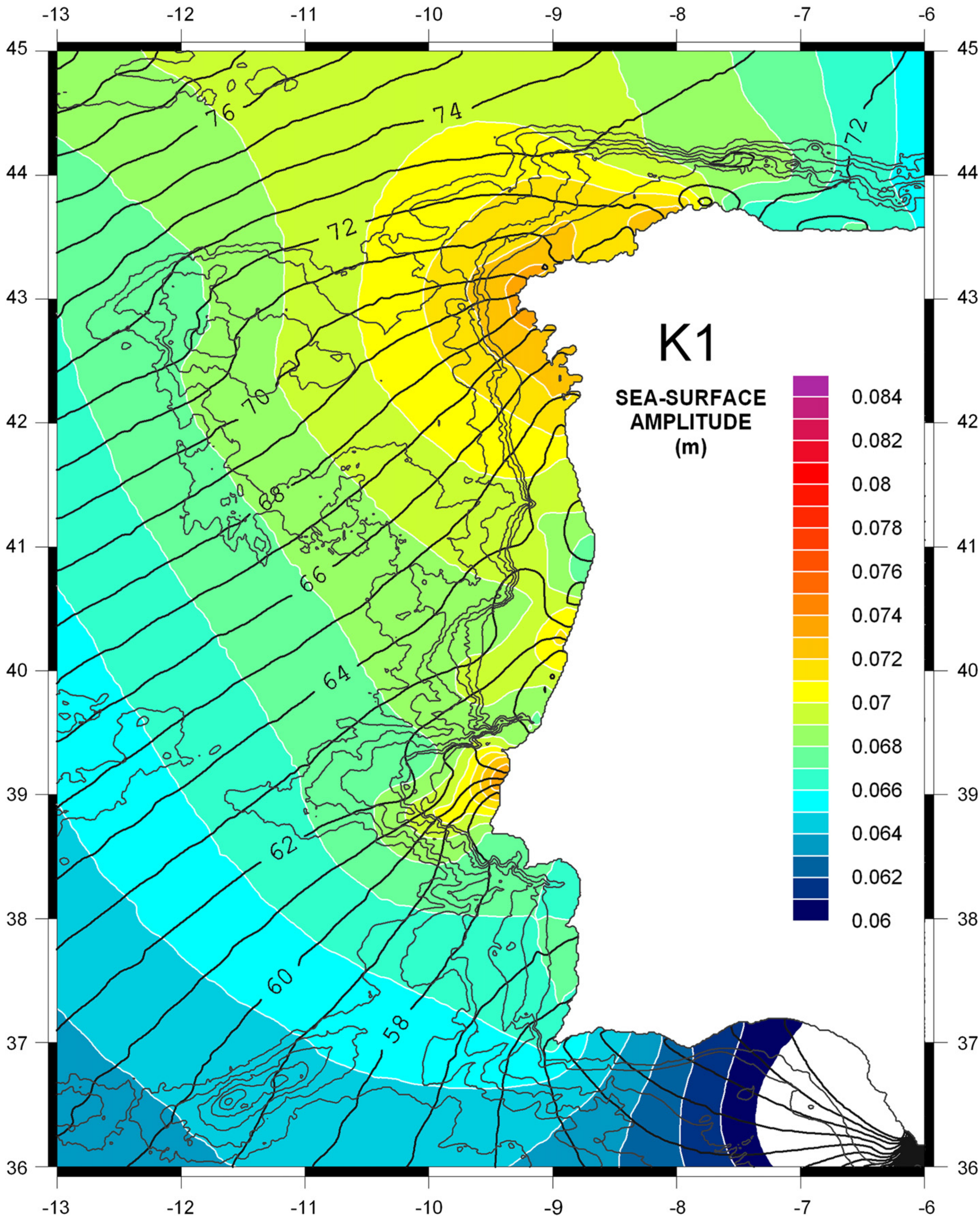

Fig. 12. K1 sea-surface amplitude chart. Amplitude (m) is represented by the colour contour and phase (degrees referenced to GMT) by black line contour. Isobaths of 200 m, 500 m, 1000 m, 2000 m, 3000 m and 4000 m were added to help interpretation.

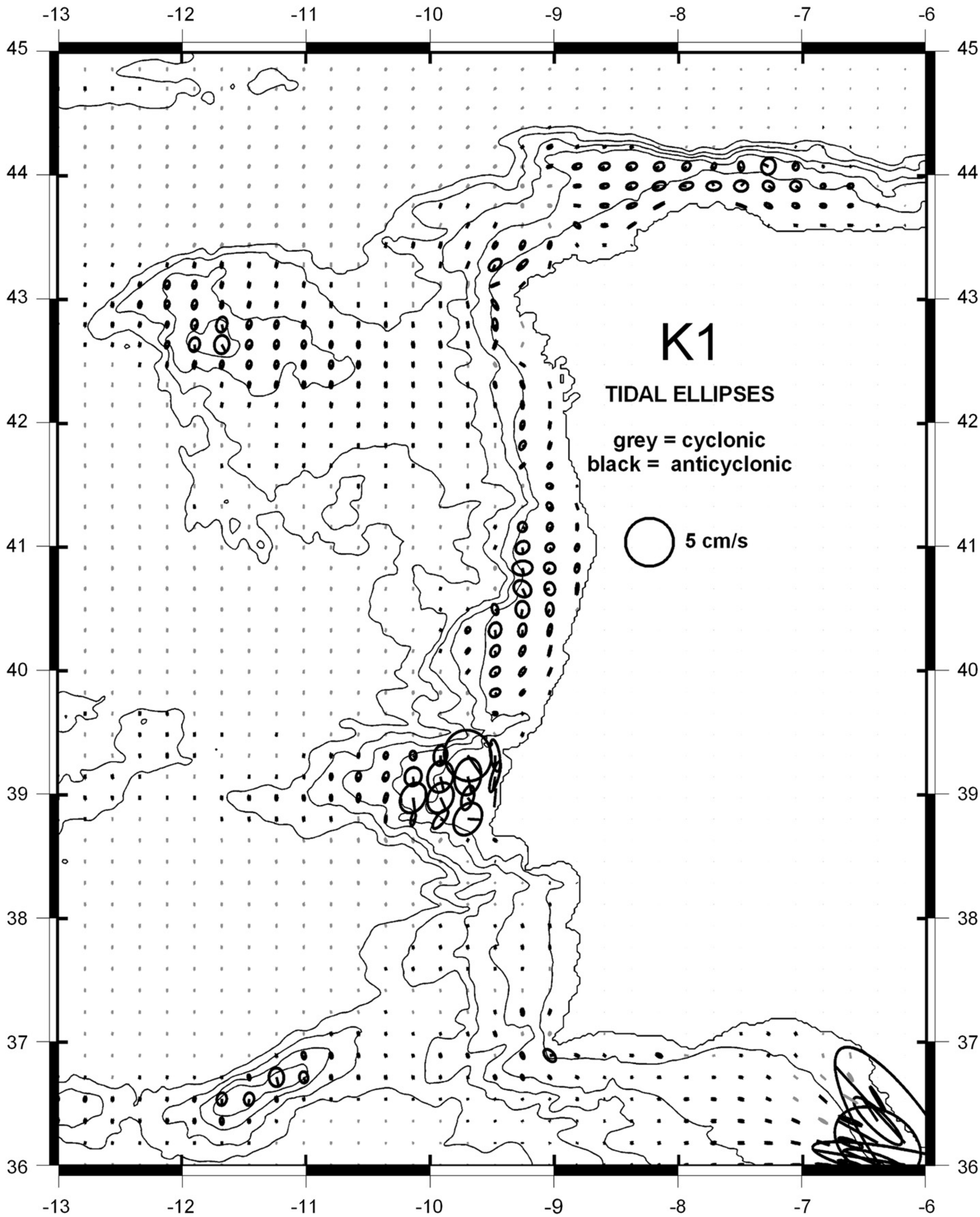

Fig. 13. K1 tidal ellipses map. The grey ellipses represent cyclonic rotation and the bold ellipses anti-cyclonic. The polar axis, traced inside each ellipse, represents the velocity phase and translates the M2 velocity vector at the same instance. Isobaths of 200 m, 500 m, 1000 m, 2000 m, 3000 m and 4000 m were added to help interpretation.

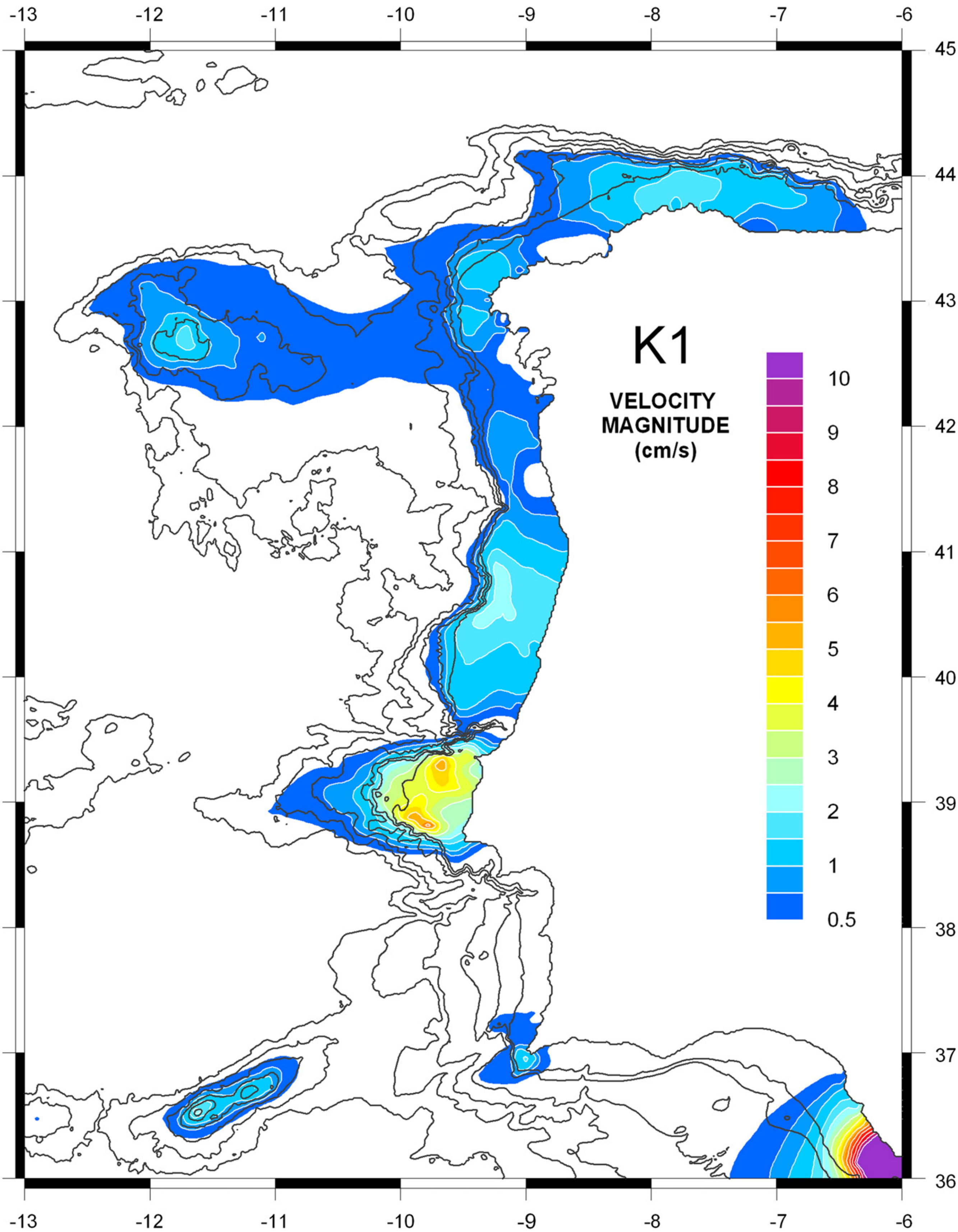

Fig. 14. K1 barotropic current velocity map. The maximum M2 velocities (cm.s^{-1}) are illustrated by the tidal ellipse semi-major axis magnitude. Isobaths of 200 m, 500 m, 1000 m, 2000 m, 3000 m and 4000 m were added to help interpretation.

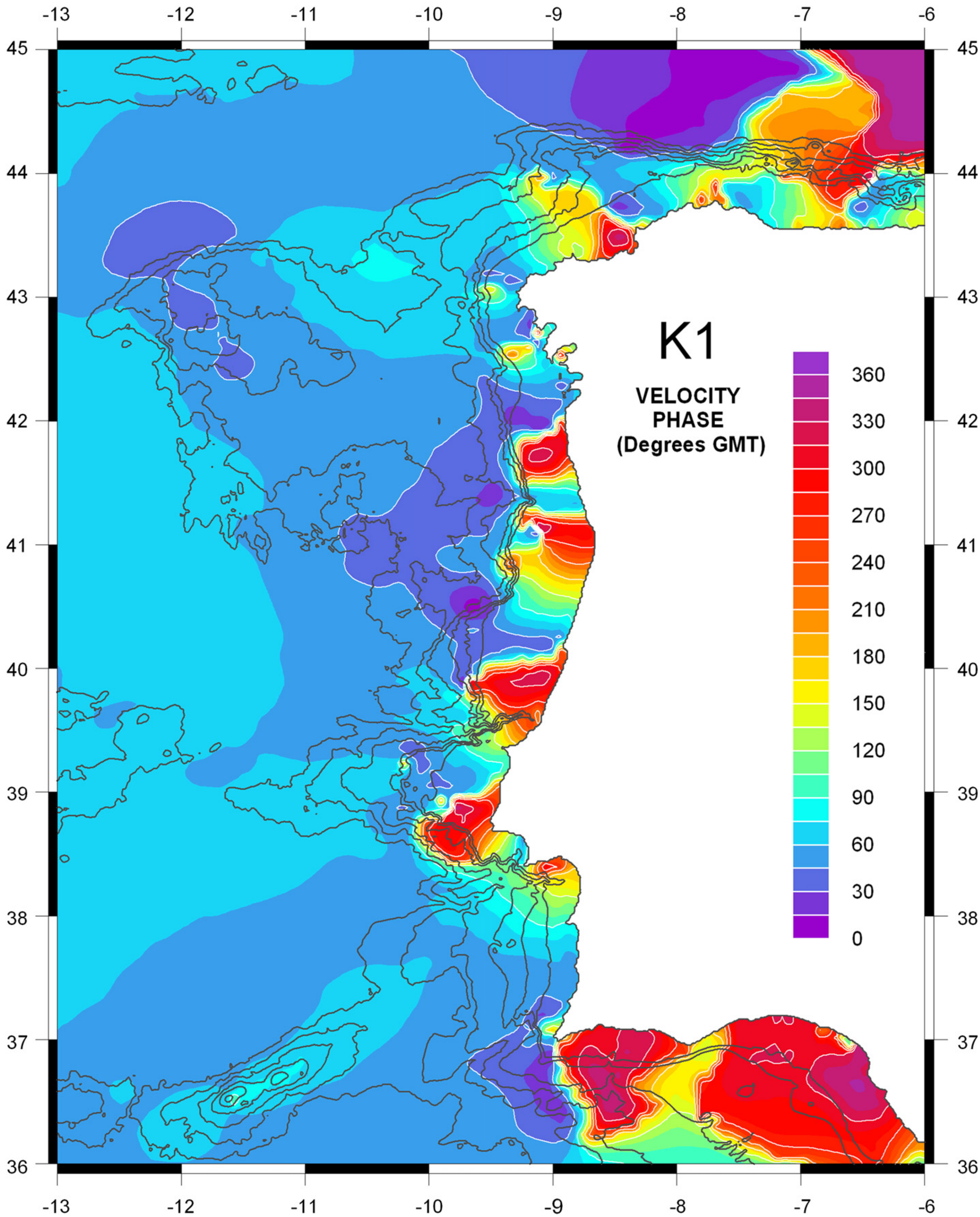

Fig. 15. K1 barotropic current velocity phase map. This corresponds to the phase lag of the maximum current behind the maximum tidal potential of M2 (degrees referenced to GMT). Isobaths of 200 m, 500 m, 1000 m, 2000 m, 3000 m and 4000 m were added to help interpretation.

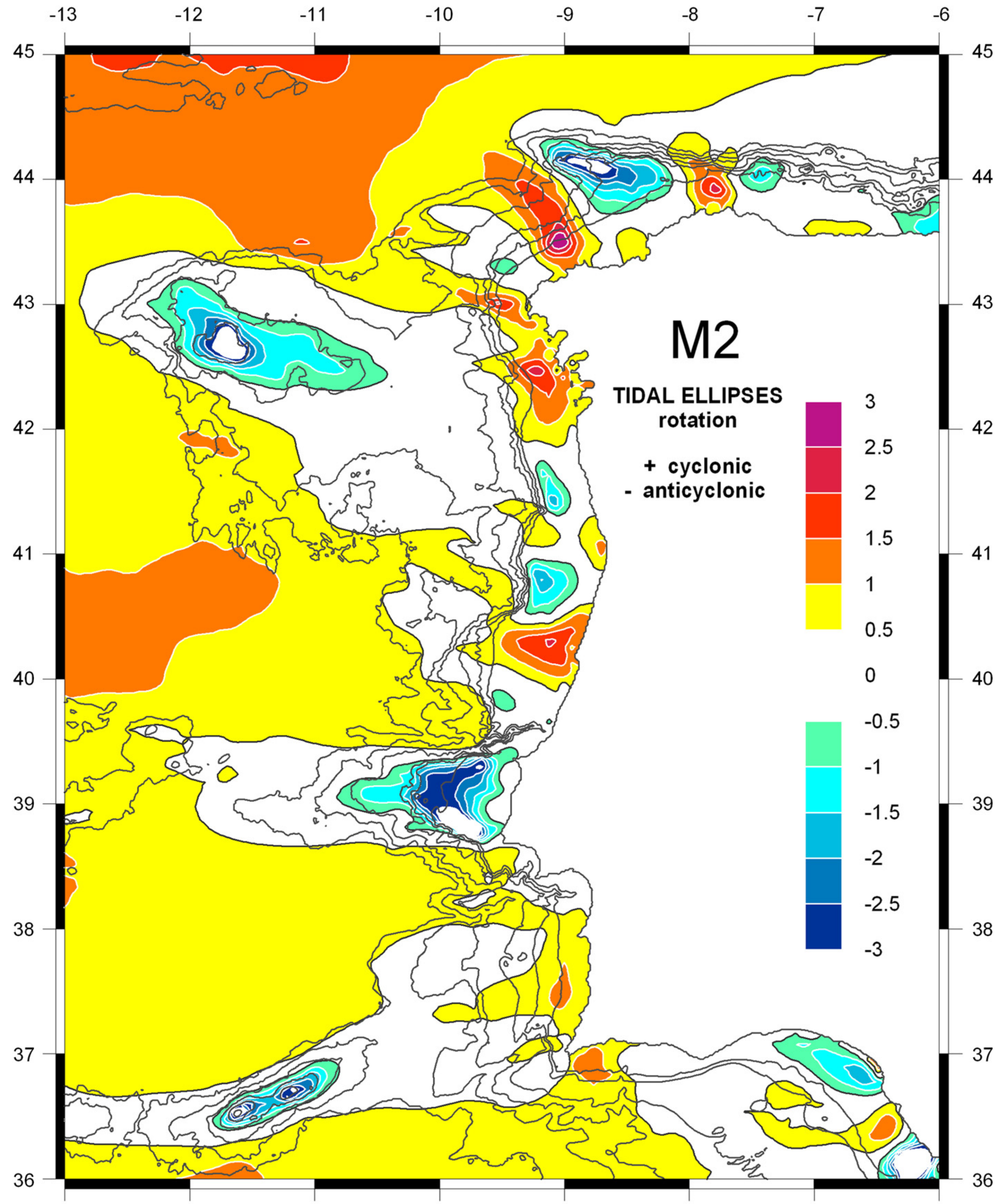

Fig. 16. M2 tidal ellipses rotation sense map. The tidal ellipse semi-minor axis sign illustrates rotation sense: positive = counter-clockwise (cyclonic); negative = clockwise (anti-cyclonic). Notice that negative values over the main topographic features are saturated in colour-scale. Isobaths of 200 m, 500 m, 1000 m, 2000 m, 3000 m and 4000 m were added to help interpretation.

Over the continental margin, the shallowing depth unbalances the Kelvin wave velocity and other modes appear, function of the forcing frequency, with wavelengths dependent of the cross-shelf profile. These modes are discussed in the next sections for each frequency domain.

5.1. Diurnal continental shelf waves

Sub-inertial trapped waves are observed along sloping margins with small offshore wave numbers, progressing along-shelf in a cyclonic sense around the deep-sea (Robinson, 1964). Continental Shelf Waves (CSW) usually calls the respective barotropic solution. Over the study region, diurnal tides are sub-inertial forcing frequencies ($\omega < f$) and can be source of these discrete sub-inertial trapped modes. This scenario is real for latitudes higher than 30° N, where f equals the diurnal tidal frequency and increases its value towards the North.

Model results suggested the presence of diurnal CSW, trapped along the West-Iberian margin, from the Tagus Plateau (39º N) towards the North. This suggestion was based on the small-scale spatial variability of the diurnal sea-surface amplitudes (large wave number structures) confined along the Portuguese northern shelf (Fig. 12). The same variability was shown in the current velocity magnitude (Fig. 14) and current velocity phase (Fig. 15). The generation seems to be linked to the abrupt coastal bathymetry features since they represent important obstacles to the tidal wave propagation. Fortunato et al. (2002) studied numerically this hypothesis and pointed out the topographic interception of the Tagus Plateau as the trigger of the observed CSW. These authors noticed also the importance of the shelf width and slope strength in the growing amplitude of the trapped wave mode.

To test the previous deductions and to validate present model results, simple analytical approach (Larsen, 1969) was applied to calculate the CSW long-shore wave number, k, and to verify it's trapping condition. The northern Portuguese margin was simplified into a step shelf of constant depth ($h_1 = 200$ m) bounded by a straight coastline and a flat abyssal plain ($h_2 = 4000$ m). The shelf width was set to vary from $L = 30$ km to $L = 50$ km. The analytical dispersion relationship turns into:

$$\frac{\omega}{f} = -\frac{h_2 - h_1}{h_1 + h_2 \coth(kL)} \tag{7}$$

The local scaled K1 frequency is $[\omega/f\,] \sim 0.78$ and the horizontal scale length, L, limited by the shelf width (verified by Fig. 15). Applying Eq. (7) to these shelf characteristics, the CSW long-shore wave number varies from $k = -3.54 \times 10^{-5}$ rad.m^{-1} ($L = 30$ km) to $k = -2.12 \times 10^{-5}$ rad.m^{-1} ($L = 50$ km). This means that equivalent wavelengths vary from $\lambda = 170$ km ($L = 30$ km) to $\lambda = 230$ km ($L = 50$ km). The observed wavelengths were taken from the numerical solution, ranging from 100 to 200 km. These lengths were estimated from the spatial scales presented in the phase of the diurnal tidal currents simulated over the northern Portuguese shelf (Fig. 15). Both analytical and numerical values are of the same order, confirming the proper simulations of CSW. The negative sign of k reflects right bounded wave propagation. The wide wavelength interval shows how sensitive the CSW solution is to the shelf width, along irregular continental margins. The differences between the analytical and numerical estimations show that the step shelf approach is not enough to accurately characterise the observed CSW structures. Other approaches, like the use of exponential shelf profiles, can be explored to obtain better results (Buchwald and Adams, 1968; Fortunato et al., 2002).

The trapping condition was verified since the scaled frequency is always smaller than the unit ($\omega < f$) and the right hand side of Eq. (5) ranges from 1 to ∞.

The model highlighted different CSW amplitudes, extending from the Tagus Plateau to the Galician shelf. This behaviour seems to be related to other existent topographic features along this margin, as submarine valleys (negative shelf width anomalies) and promontories (positive shelf width anomalies). This issue should be addressed in a future work, in order to understand how the varying 2D topography modulates locally the sub-inertial trapped waves modes.

5.2. Semidiurnal waves shelf variability

The cotidal charts of the semi-diurnal constituents suggested a large-scale tidal wave propagating in Kelvin mode, along the West-Iberian margin (Fig. 8). However, tidal velocity maps showed small-scale structures over the continental margin with wavelengths of about 100 km (Figs. 10 and 11). These structures seem trapped by shelf-width anomalies, creating the impression of a “wave-like” configuration (Fig. 16).

In nature, besides the fundamental Kelvin mode, other coastal super-inertial modes exist: edge waves and modified Poincaré waves. Edge waves are topographic trapped modes with large wave number (small-scale oscillations). Poincaré waves are free modes with small wave number, modified by topography (large-scale waves). The trapping condition Eq. (5) splits these coastal wave modes in distinct [ω, k] domains (Huthnance, 1975). For an imposed super-inertial frequency there is a continuum of Poincaré waves solutions and a discrete sequence of unique edge-wave modes. The number of possible existing edge-wave modes is function of the wave frequency. For the same frequency, the Kelvin mode arises at higher wave number and consequently becomes the smaller wavelength trapped at the coast. This statement sets aside the hypothesis of small-scale semi-diurnal trapped waves simulated over the West-Iberian margin.

Rosenfeld and Beardsley (1987) encountered a similar behaviour when analysing tidal velocity observations along the Californian shelf. They proposed a bumpy coastline as an inductor of velocity differences over short distances (<100 km). Similar to the present simulation, the resulting effect was more visible in the velocity field than in the sea-surface amplitude. The spatial variability acquired a wavelength of the same order of magnitude as the distance between coastline bumps.

Several shelf width anomalies, like submarine canyons and shelf spurs are evenly spaced along the West-Iberian margin. The along-shelf distance between these features vary from 40 to 100 km. The small-scale velocity structures, observed in the ellipse magnitude (Fig. 10), phase (Fig. 11) and rotation sense (Fig. 16) exhibit similar wavelengths. These deductions suggest that the “wave-like” configuration do not result from trapped wave mode, but is consequence of along-shelf wave modulation by evenly spaced bathymetry features.

6. Barotropic forcing term

One of the present work's main objectives was the improvement of the barotropic tide regional simulation, to be used in future numerical modelling of the subsequent baroclinic modes, when water-column stratification is introduced. Internal tides are generated by small-scale horizontal pressure gradients created by alternate barotropic tidal flow over steep topography. This mechanism can be scaled locally by the respective forcing term, function of the current velocity magnitude and bathymetry slope:

$$\frac{1}{H} U \cdot \nabla H \quad or \quad \left[\frac{U_n \cos(\omega_n t - \phi_{Un})}{H} \frac{\partial H}{\partial x} + \frac{V_n \cos(\omega_n t - \phi_{Vn})}{H} \frac{\partial H}{\partial y} \right] \tag{8}$$

Barotropic velocity was decomposed in orthogonal component magnitudes (U, V) and by tidal constituents (n). The forcing term only accounted for super-inertial constituents, since internal waves are limited in frequency by [$N < \omega_n < f$], where N represents the buoyancy frequency. Semi-diurnal polychromatic simulations (M2, S2, N2

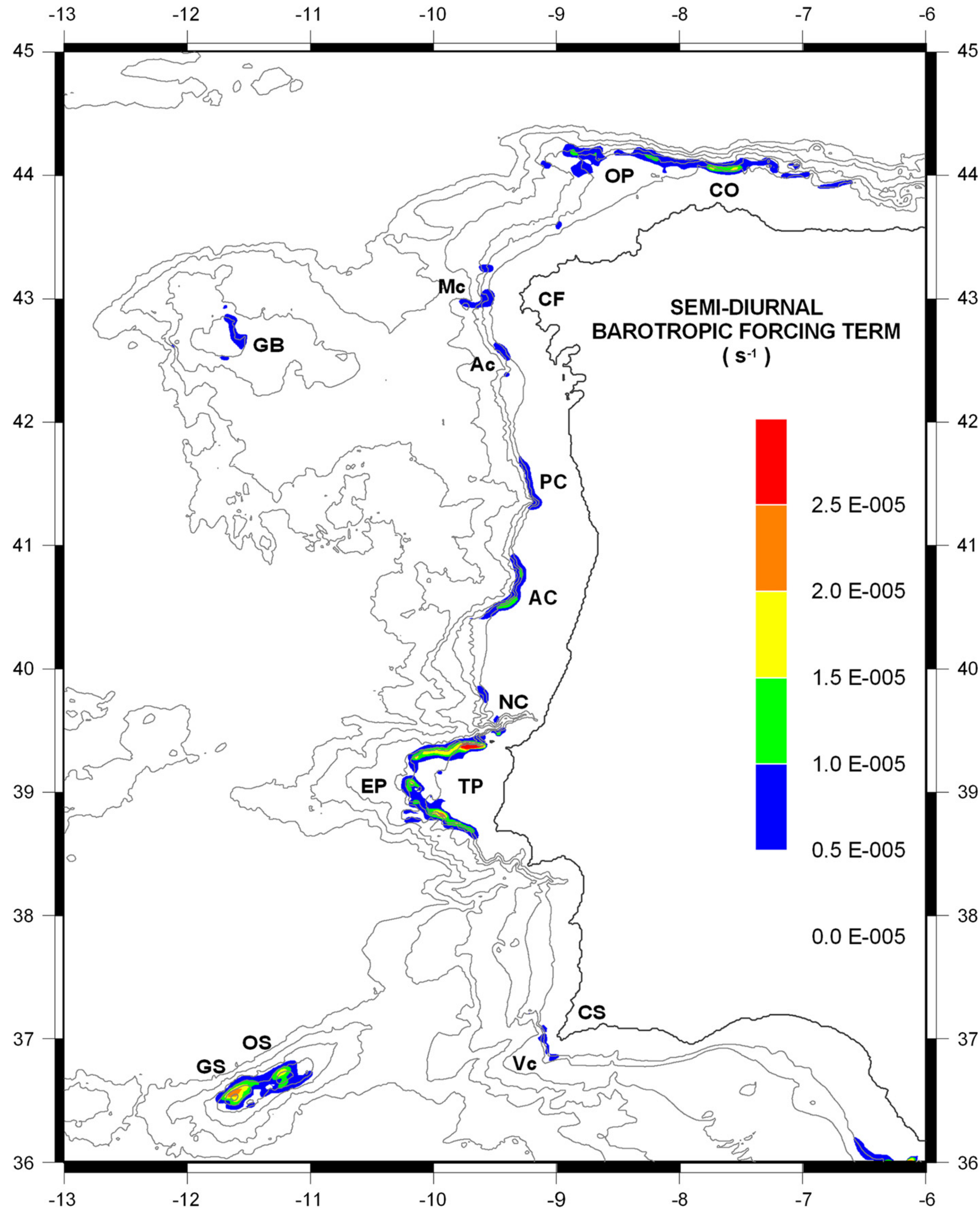

Fig. 17. Semi-diurnal barotropic forcing term map (s^{-1}). Isobaths of 200 m, 500 m, 1000 m, 2000 m, 3000 m and 4000 m were added to help interpretation. Internal tide generation "hotspots" are pointed out by the following symbols: TP (Tagus Plateau); EC (Estremadura promontory); OP (Ortegal promontory); NC (Nazaré canyon); AV (Aveiro canyon); PC (Porto canyon); Ac (Arosa canyon); Mc (Murgia Canyon); Vc (S. Vicente canyon); GB (Galician banks); CO (cape of Ortegal); CF (cape of Finisterra); CS (cape of Sagres) and the Gorringe banks are presented by GS (Gettysburg seamount) and OS (Ormonde seamount).

and K2) were performed in order to calculate the barotropic forcing term set up by the tide along the West-Iberian margin. As expected, maxima values were found along the shelf-break of the major topographic reliefs faces (Fig. 17). These locations constitute internal tide generation "hotspots", where the barotropic tide transfers energy to higher order vertical modes (baroclinic tide).

Most of the identified "hotspots" were already pointed separately in literature. The northern continental slope of the Galician margin reveals several maximal values, primarily at the promontory of Ortegal (Azevedo et al., 2006; Pichon and Correard, 2006) reaching $2.0\times10^{-5}\,s^{-1}$. Around the cape of Finisterra, other areas evidence important forcing term values, like the edges of the submarine canyons of Murgia and Arosa. Offshore, Galicia banks are also known sources of internal tide generation.

Along the northern Portuguese shelf, two major submarine valleys (Porto and Aveiro) highlight an extensive shelf-break belt (200 to 500 m depth) where the forcing term is considerably high (reaching $1.5\times10^{-5}\,s^{-1}$). In the central region of the West-Iberian margin, two huge topographic features (Nazaré submarine Canyon and the Estremadura promontory) imprint the higher forcing values found ($\sim3.0\times10^{-5}\,s^{-1}$). Several "hotspots" are displaced around the Tagus Plateau shelf-break. This fact results from significant tidal velocity amplification (verified earlier) over very strong topographic slopes, as the northern and southern faces of the Estremadura promontory. The achieved barotropic forcing values are comparable to the ones estimated at French slope in Bay of Biscay and are higher than the values estimated at the faces of the promontory of Ortegal (Pichon and Correard, 2006). The Nazaré canyon rim reveals also measurable forcing values, already suggested by Quaresma et al. (2007). In the southern Portuguese margin, other "hotspots" were found offshore the cape of Sagres, where an important submarine canyon comprises strong slopes (S. Vicente canyon).

One very strong "hotspot" is revealed southwest of the Iberian margin (36.5° N/11.5° W). This corresponds to the Gorringe bank where the Gettysburg and Ormonde seamounts rise from the abyssal plain to depths of 25 m and 48 m respectively. Here, the M2 flow is blocked and velocities punctually exceed 10 cm.s^{-1} in the middle of Atlantic Ocean.

The precedent evaluation highlights the main baroclinic tide generation spots at the West-Iberian margin. However, other smaller areas have been proposed in literature, based on satellite Syntactic Aperture Radar imagery (SAR) interpretation (Jeans and Sherwin, 2001; Sherwin et al., 2002; Small, 2002). The topographic slope, calculated in Eq. (8), is function of the adopted model grid resolution (1 arc-minute). This constraint filters the spatial distribution of the barotropic forcing term. Small-scale topographic slopes are not represented by the present model and can be also sources of internal tidal waves (observed in SAR images as internal solitary wave surface signatures).

7. Summary

A circulation numerical model was successfully applied to simulate the barotropic tide along the West-Iberian margin. A new DTM was constructed and validated by model results. The tidal residual current was suitably used as a proxy to tune the viscosity parameterization in the numerical model. Astronomical tide-raising forces, acting regionally, were taken into account by adding the gravitational tidal gradient force into HYCOM momentum equations.

Eight principal harmonics were accurately modelled together by forcing a polychromatic tidal spectrum at the open boundaries. The best semi-diurnal results were obtained when forcing the model with NEA2004 (K2 constituent was the exception) and the best diurnal by forcing TPXO7.2. The model was evaluated by a consistent set of *in situ* observations (11 Tide-gauges and 4 current profile time-series), spaced along the domain. The results attest an accuracy improvement from previous references.

Spatial analysis of the tide shows that its principal harmonics can be grouped in super and sub-inertial classes. Within each class, the regional tidal amplitude and velocity distribution exhibit similar behaviour. The model, in agreement with analytical analysis, reproduces diurnal continental shelf waves along the northern Portuguese shelf. Small-scale semi-diurnal variability is also present. These structures were evaluated and pointed out as being a result of tidal wave modulation by shelf width anomalies, imposed by coastal bathymetry features.

The barotropic forcing term was calculated along the West-Iberian margin and the main internal tide "hotspots" were revealed, namely over the major submarine canyons and promontories, as well as over nearby seamounts. The numerous hotspots and their significant forcing term values suggests strong internal tide activity along the West-Iberian margin, already observed by cited authors.

Acknowledgements

The present study is part of Luis Quaresma PhD work, taking place at the SHOM (French Service Hydrographique et Océanographique de la Marine), followed by UBO (French Université de Bretagne Occidentale) and HIDROGRAFICO (Portuguese Instituto Hidrográfico) and co-supported by FCT (Portuguese Fundação para a Ciência e Tecnologia). The authors would like to give special thanks to *Bernard Le Cann* for the important discussions on the subject. Also to HIDROGRAFICO, SHOM, PUERTOS DEL ESTADO and IFREMER for the available data access.

References

Amante, C., Eakins, B.W., 2009. ETOPO1 1 Arc-minute Global Relief Model: Procedures, Data Sources and Analysis. NOAA Technical Memorandum NESDIS NGDC, 19 pp.

Azevedo, A., Da Silva, J.C.B., New, A.L., 2006. On the generation and propagation of internal solitary waves in the southern bay of Biscay. Deep Sea Research 53 (6), 927–941.

Battisti, D.S., Clarke, A.J., 1982. A simple method for estimating barotropic tidal currents on continental margins with specific applications to the M2 tide off the Atlantic and Pacific coasts of the United States. Journal of Physical Oceanography 12, 8–16.

Bleck, R., 2002. An oceanic general circulation model framed in hybrid isopycnic-cartesian coordinates. Ocean Modelling 4, 55–88.

Bleck, R., Boudra, D.B., 1981. Initial testing of a numerical ocean circulation model using a hybrid (quasi-isopycnic) vertical coordinate. Journal of Physical Oceanography 11, 755–770.

Bleck, R., Smith, L., 1990. A wind-driven isopycnic coordinate model of the north and equatorial Atlantic Ocean. 1.Model development and supporting experiments. Journal of Geophysical Research 95C, 3273–3285.

Buchwald, V.T., Adams, J.K., 1968. The propagation of continental shelf waves. Proceedings of the Royal Society A 305, 235–250.

Da Silva, J.C., Ermakov, S.A., Robinson, I.S., Jeans, D.R., Kijashko, S.V., 1998. Role of surface films in ERS SAR signatures of internal waves on the shelf, 1, short-period internal waves. Journal of Geophysical Research 103, 8009–8031.

Egbert, G., Bennett, A., Foreman, M., 1994. TOPEX/ POSEIDON tides estimated using a global inverse model. Journal of Geophysical Research 99, 24821–24852.

Fanjul, E., Gómez, B., Sánchez-Arévalo, I., 1997. A description of the tides in the Eastern North Atlantic. Progress in Oceanography 40, 217–244.

Fortunato, A., Pinto, L., Oliveira, A., Ferreira, J., 2002. Tidally generated shelf waves off the western Iberian coast. Continental Shelf Research 22, 1935–1950.

Huthnance, J.M., 1975. On trapped waves over a continental shelf. Journal of Fluid Mechanics 69, 689–704.

Jeans, D.R.G., Sherwin, T.J., 2001. The variability of strongly non-linear solitary internal waves observed during an upwelling season on the Portuguese Shelf. Continental Shelf Research 21, 1855–1878.

Larsen, J.C., 1969. Long waves along a single-step topography in a semi-infinite uniformly rotating ocean. Journal of Marine Research 27, 1–6.

LeCann, B., 1990. Barotropic tidal dynamics of the Bay of Biscay shelf: observations, numerical modelling and physical interpretation. Continental Shelf Research 10 (8), 723–758.

Lyard, F., Lefevre, F., Letellier, T., Francis, O., 2006. Modelling the global ocean tides: modern insights from FES2004. Ocean Dynamics 56, 394–415.

Marta-Almeida, M., Dubert, J., 2006. The structure of tides in the western Iberian region. Continental Shelf Research 26, 385–400.

Morel, Y., Baraille, R., Pichon, A., 2008. Time splitting and linear stability of the slow part of the barotropic component. Ocean Modelling 23 (3–4), 73–81.

Pairaud, I.L., Lyard, F., Auclair, F., Letellier, T., Marsaleix, P., 2008. Dynamics of the semi-diurnal and quarter-diurnal internal tides in the Bay of Biscay. Part 1: Barotropic tides. Continental Shelf Research 28, 1294–1315.

Pawlowicz, R., Beardsley, B., Lentz, S., 2002. Classic tidal harmonic analysis including error estimates in MATLAB using T_TIDE. Computers and Geosciences 28, 929–937.
Pichon, A., Correard, S., 2006. Internal tides modeling in the bay of Biscay. Comparisons with observations. Scientia Marina 70S1, 68–88.
Prandle, D., 1997. The influence of bed friction and vertical eddy viscosity on tidal propagation. Continental Shelf Research 17, 1367–1374.
Quaresma, L.S., Vitorino, J., Oliveira, A., DaSilva, J., 2007. Evidence of sediment resuspension by nonlinear internal waves on the western Portuguese mid-shelf. Marine Geology 246, 123–143.
Ray, R.D., 1998. Ocean Self-Attraction and Loading in Numerical Tidal Models. Marine Geodesy 21, 181–192.
Robinson, A.R., 1964. Continental shelf waves and the response of sea level to weather systems. Journal of Geophysical Research 69, 367–368.
Robinson, I.S., 1981. Tidal vorticity and residual circulation. Deep Sea Research 28A (3), 195–212.
Rosenfeld, L.K., Beardsley, R.C., 1987. Barotropic semi-diurnal tidal currents off Northern California during the Coastal Ocean Dynamics Experiment (CODE). Journal of Geophysical Research 92, 1721–1732.
Sauvaget, P., David, E., Guedes Soares, C., 2000. Modelling tidal currents on the coast of Portugal. Coastal Engineering 40, 393–409.
Sherwin, T.J., Vlasenko, V.I., Stashchuk, N., Jeans, D.R.G., Jones, B., 2002. Along-slope generation as an explanation for unusually large internal tides. Deep-Sea Research I 49, 1787–1799.
Simon, B., 2007. La Marée Océanique Côtière. Inst. Oceanogr., Paris. 443 pp.
Small, J., 2002. Internal tide transformation across a continental slope off Cape Sines, Portugal. Journal of Marine Systems 32, 43–69.